2011

Bio-Functionalized Clay Nanoparticles for Wound Healing Applications

Christopher Anthony Vaiana
Wright State University

BIO-FUNCTIONALIZED CLAY NANOPARTICLES FOR WOUND HEALING APPLICATIONS

A thesis submitted in partial fulfillment

of the requirements for the degree of

Master of Science

By

Christopher A. Vaiana

B.A., SUNY Binghamton, 2007

2011

Wright State University

WRIGHT STATE UNIVERSITY
SCHOOL OF GRADUATE STUDIES

May 10, 2011

I HEREBY RECOMMEND THAT THE THESIS PREPARED UNDER MY SUPERVISION BY *Christopher Vaiana* ENTITLED *Bio-functionalized Clay Nanoparticles for Wound Healing Applications* BE ACCEPTED IN PARTIAL FULFILLMENT OF THE REQUIREMENTS FOR THE DEGREE OF *Master of Science*

_____
Madhavi P. Kadakia, Ph.D.
Thesis Director

_____
Steven J. Berberich, Ph.D.
Department Chair,

Committee on
Final Examination

_____
Madhavi P. Kadakia, Ph.D.

_____
Rajesh R. Naik, Ph.D.

_____
Lawrence J. Prochaska, Ph.D.

_____
Andrew Hsu, Ph.D.
Dean, School of Graduate Studies

Abstract

Vaiana, Christopher A., M.S., Department of Biochemistry and Molecular Biology, Wright State University, 2010
Bio-functionalized Clay Nanoparticles for Wound Healing Applications

Wound healing is a complex, multi-step process that can be summarized into three stages, namely hemostasis and inflammation, proliferation, and finally tissue remodeling. Battlefield wound healing demands rapid hemostasis using clotting or cauterizing agents to immediately limit blood loss, but this occurs at the expense of proper tissue repair beyond hemostasis. Layered silicate clays such as kaolin and montmorillonite (MMT) have been previously shown to induce blood clotting due to their ability to form charged interactions with clotting factors. The charge characteristics of sodium MMT (Na-MMT) also enable functionalization with active biomolecules. Herein we first functionalize three types of alumoinosilicate clays, namely Na-MMT, kaolin, and halloysite with horseradish peroxidase (HRP) as a model system with which to study the binding and biological activity of biomolecules bound to MMT. We then functionalized Na-MMT with epidermal growth factor (EGF) via ion exchange reaction to create a nanocomposite (MMT-EGF) with EGF occupying approximately 0.12 % of the Na^+ exchange sites and conduct biochemical analysis of keratinocytes after treatment with MMT-EGF. Our results demonstrate that EGF immobilized on MMT retains the ability to activate the epidermal growth factor receptor (EGRF), causing phosphorylation of the AKT and MEK1 pathways, as well as upregulation of its downstream target gene expression involved in cell growth and migration.

This study also shows that like EGF, MMT-EGF treatment can stimulate cell migration *in vitro*, which is dependent on ERK1/2 phosphorylation.

Table of Contents

List of Figures

List of Tables

Acknowledgements

I would like to express heartfelt gratitude toward my advisors Dr. Madhavi Kadakia and Dr. Rajesh Naik, whose unfaltering discipline, encouragement, and wisdom have made this work possible, and who have set for me a precedent of excellence and a true love of research, which I shall carry with me forever – thank you for all you have done.

I would like to thank the members of the Kadakia lab past and present, especially Katie Leonard, Andy Whitlatch, and Ramma Kommagani, as well as the members of the Naik lab, especially Lawrence Drummy and Kristi Singh, for their contributions not only to this work, but to my growth as a person and researcher.

I would like to thank Dr. Athanasios Bubulya and Dr. Richard Vaia for their sincere guidance throughout this project, and Dr. Lawrence Prochaska as a member of my thesis committee – thank you for making this effort possible.

I would finally like to thank my parents, family, and friends whose love, support, patience, and encouragement have made me the person I am today.

I. Introduction

A. An overview of epidermal wound healing

Skin is the largest organ in the human body, composed of an outer epidermis and inner dermis, and serves many functions including protection from the environment, fluid maintenance, and thermal regulation (Madison). Because the epidermis is our body's primary protection against the external environment, it is susceptible to frequent wounding, and therefore is equipped with a complex healing mechanism. Wound healing is a multi-staged cellular response, resulting in the activation of several overlapping cascades of protein activity (Martin). The different stages of wound healing can be classified as: hemostasis and inflammation, proliferation, and tissue remodeling as depicted in Figure 1 (Stadelmann, Digenis and Tobin; Beanes et al.). Hemostasis (blood clotting) is the body's immediate response to limiting blood and fluid loss by sealing the wound shut. During this stage, vasoconstriction and platelet aggregation begin clotting, followed by the activation of several events making up the coagulation cascade. The release of growth factors initiates the proliferative stage, where angiogenesis, collagen scaffold formation, fibroplasia, and epithelialization occur (Singer and Clark). This proliferation stage begins within hours of hemostasis, and may last weeks to months depending on the severity of the wound (Beanes et al.). Finally the process ends with tissue remodeling which may take years to fully complete. Because of the inherent complexity of wound healing, it is difficult to design new technologies that can enhance more than one stage of the healing process.

Figure 1. Schematic representation of the cutaneous wound healing process. After injury, stage 1 of the wound healing process is the aggregation of platelets and activation of the coagulation cascade, resulting in the formation of a fibrin clot. The release of growth factors initiates stage 2 where a collagen scaffold is laid down and fibroblast proliferation across the wound area occurs. The final stage, tissue remodeling, completes the process as reorganization of the new tissue takes place.

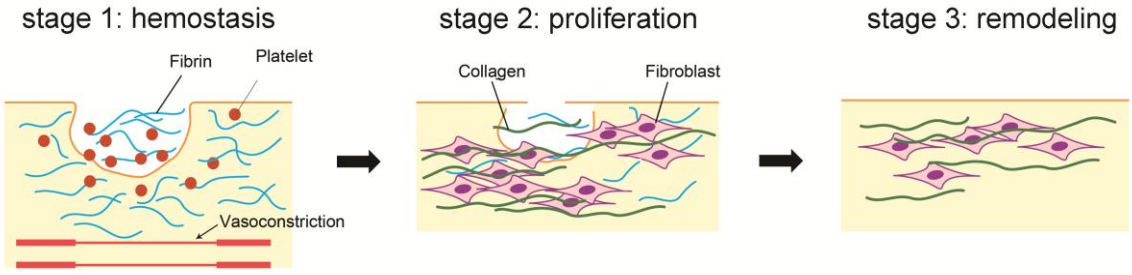

Adapted from Beanes SR, et al. Expert Rev Mol Med, 2003 Mar;5(8):1-22.

B. The structure and function of epidermal growth factor and its receptor.

Epidermal growth factor (EGF) is a single-chain, 53 amino acid residue peptide involved in the regulation of cell proliferation and differentiation via the EGF receptor (EGFR) (Ogiso et al.). EGF is one of several ligands that activate members of the ErbB receptor family, which includes EGFR (or ErbB1), ErbB2 ErbB3, and ErbB4 (Danielsen and Maihle). These membrane-spanning receptors, which are made up of an extracellular ligand-binding region, a trans-membrane region, and an intracellular region, have been shown to play a role in the regulation of cell replication, movement, and survival. The extracellular region of EGFR consist of 4 domains (I – IV) with EGF docking between domains I and III (Ogiso et al.). While it is known that activation of EGFR involves dimerization of two inactive EGFR monomers due to the docking of two EGF molecules, the exact mechanism by which this occurs is not completely known. Three distinct hypotheses exist to explain this mechanism; one hypothesis suggests ligand (EGF) dimerization facilitates the dimerization of the receptors, supported by the observation of the interaction between two asymmetric EGF molecules in X-ray crystallography; a second hypothesis suggests a receptor-mediated mechanism, where the binding of EGF to EGFR induces a conformational change in EGFR that allows dimerization of two EGFR monomers; and a third hypothesis suggests a bivalent interaction between a single EGF molecule and two EGFR monomers (Lemmon et al.; Lu et al.; Ogiso et al.). The dynamics of EGF-EGFR interaction may play an important role in designing different EGF-based delivery mechanisms for wound healing applications.

C. The role of epidermal growth factor in wound healing

EGF is one of the major growth factors that stimulate cell proliferation and motility during tissue regeneration (Hudson and McCawley; Koivisto et al.; Liang et al.). The use of EGF and other growth factors to stimulate cell proliferation during wound healing has been repeatedly demonstrated with varying success (Choi, Leong and Yoo; Fu et al.). EGF acts by binding and activating EGFR, thereby communicating growth signals through various protein cascades (Langlands, Down and Kealey; Marques et al.). One major pathway starts with phosphoinositide 3-kinase (PI3K). Phosphorylation of PI3K by activated EGFR subsequently leads to activation of AKT pathway, a major conduit of PI3K pro-growth signals (Hennessy et al.). AKT activation leads to phopshorylation of several downstream targets which promote cell survival. For example, AKT phosphorylates and activates mammalian target of rapamycin (mTOR) which leads to translation of growth proteins such as p-70 (S6 kinase) and phosphorylation of S6 (Vander Haar et al.). AKT also directly inhibits glycogen synthase kinase 3β (GSK3β) through phosphorylation, thereby inhibiting the degradation of β-catenin, resulting in transcription of c-JUN and other pro-growth genes (Jope and Johnson). EGFR also promotes cell growth by means of mitogen activated protein kinase (MAPK) pathways such as ERK1/2 via the RAS-RAF-MEK cascade (Seger and Krebs). Interestingly, ERK activation has been shown to play a major role in epithelial cell migration during wound healing (Sharma, He and Bazan; Matsubayashi et al.). Overexpression of EGFR and other ErbB receptors play a major role in some cancers, and have been shown to

promote their survival by suppression of apoptosis via PI3K/AKT/Bad or MAPK/RSKS/Bad interactions as depicted in Figure 2 (Danielsen and Maihle; Bose et al.).

Research in the use of growth factors for treatment of different types of wounds has gained momentum over the last several years. Within the last decade or so, several growth factors including EGF, basic fibroblast growth factor (bFGF), and platelet-derived growth factor (PDGF) have gained United States FDA approval for wound healing (Fu et al.). Healing of chronic wounds shows significant improvement with growth factor treatment, although several challenges still exist, such as the tendency of proteases activity in the wound area to destroy much of the growth factors upon treatment (Hardwicke et al.).

D. Structure and applications of layered aluminosilicate clays

Aluminosilicates are abundant, natural, layered clay mineral structures composed predominantly of silicon, aluminum, and oxygen (Grim). Nanoscale layered aluminosilicates have gained momentum in advanced biomedical uses such as cell scaffolding and drug delivery (G. V. Joshi et al.; S.R. Levis and P.B. Deasy; Mehta et al.; Aguzzi et al.). Montmorillonite (MMT) is an aluminosilicate clay mineral consisting of a 2:1 structure of two outer tetrahedral silicon layers sandwiching an inner octahedral aluminum layer. MMT consists of a lamellar stack of crystalline, 1 nm thick aluminosilicate sheets.

Figure 2. Schematic representation of EGFR inhibition of apoptosis via AKT and MEK. Upon ligand binding, EGFR acts to phosphorylate and activate AKT via PI3-K and RSKS via the RAS-RAF-MEK signaling cascades. Active AKT and RSKS directly inhibit the apoptotic actions of Bad, thereby promoting cell survival.

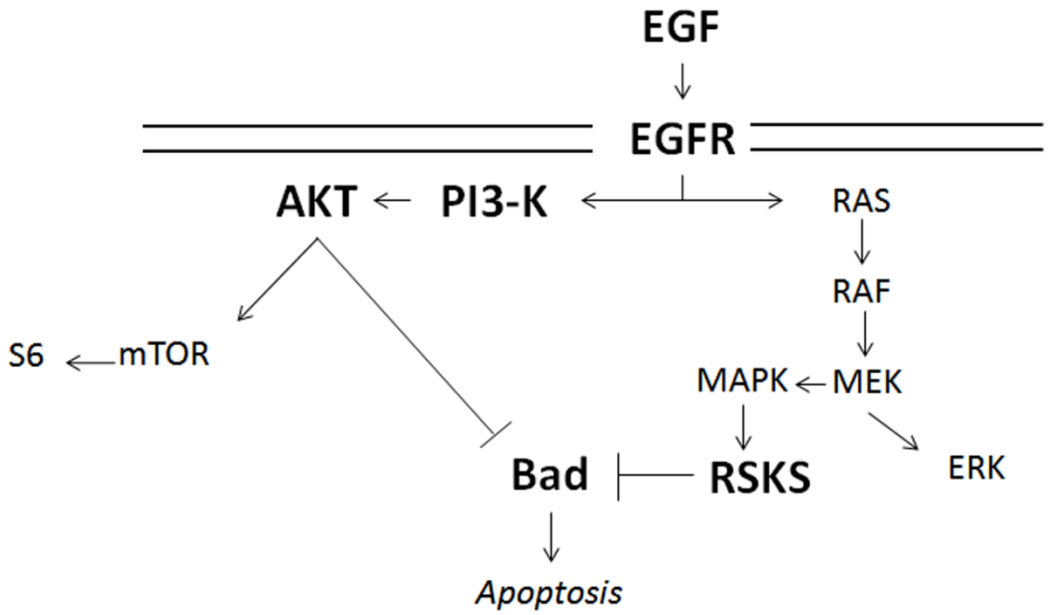
EGF
EGFR
AKT
PI3-K
RAS
RAF
S6
mTOR
MAPK
MEK
ERK
Bad
RSKS
Apoptosis

Naturally occurring cations (ie, Na^+) reside between the sheets to balance the overall negative surface charge of the MMT. In water, the lamellar stack swells producing an electrostatically stabilized dispersion of nanoscale sheets. Ingestion of MMT has been used therapeutically for the absorption of toxins in the colon and intestines (Aguzzi et al.). The ion exchange capacity of MMT enables replacement of Na^+ with other organic and inorganic cations to add functionality, spurring research into the use of MMT and other clay species as oral drug delivery agents for molecules such as 5-fluorouracil, a chemotherapeutic agent for treating colon cancer (Lin et al.).

Kaolin is another aluminosilicate clay, consisting of a 1:1 structure of a single tetrahedral silicon layer and a single octahedral aluminum layer, that has been shown for years to induce coagulation by activating clotting factor such as Hageman Factor (Factor XII) (Cochrane, Revak and Wuepper). It can be found in several ingested medicines as an antacid, and is used to mitigate diarrhea (Wald; Linare, Afonso and Rose-Brussin). Halloysite is an aluminosilicate clay with a similar chemical makeup of kaolin, but is oriented in a hollow nano tubular structure as opposed to the lamellar stacks of MMT or kaolin. Entrapment of drug molecules inside the tube for sustained drug release applications has been shown in several studies both *in vitro* and *in vivo* (S.R. Levis and P.B. Deasy; Price, Gaber and Lvov). While the functionalization of MMT with drug molecules utilizes the clay's ion exchange ability, drug loading of halloysite involves replacement of the intercalated water inside the hollow tube structure with a solution containing the molecule of choice. MMT, kaolin, and halloysite each

have unique properties that make them attractive for use in the biomedical community. Overall, the ion exchange nature, intercalation properties, and biocompatibility of clays make them ideal candidates for growth factor delivery.

E. Enzymes and their use in aluminosilicate nanocomposites.

The interest in immobilization of enzymes and other active biomolecules onto clay surfaces for use as biocatalysts ranges from basic research to industry. The isolation and immobilization of enzymes that perform a desired reaction or yield a certain product has been used in industries such as food technology, biotechnology, biomedicine, and analytical chemistry (Gopinath and Sugunan; Hartmeier). Common enzymes that have shown varying degrees of activity when immobilized include horseradish peroxidase (HRP) and glucose oxidase (GOX), among others (Lozzi et al.; Sanjay and Sugunan; Garwood, Mortland and Pinnavaia). In some cases, research groups observe a decrease in the activity of enzymes immobilized to clay surfaces (Lozzi et al.). Since the enzyme is being taken out of its natural environment, there are many external factors that may inhibit its activity such as temperature and ionic conditions. Other research groups, however, show an increase or stabilization in activity of immobilized enzymes (Sanjay and Sugunan). Enzymes function in a very crowded *in vivo* environment, and the confinement of enzymes in some porus materials has been reported to play a role in increasing enzyme activity (Dunker and Fernández). HRP is an example of a well-studied enzyme, and has been used in various applications in research, industry, and medicine today (Veitch). It was used in

this study as a model with which to study the biological activity of clay-bound biomolecules in an aqueous environment.

F. Rationale and Significance.

Research into the mechanisms behind each stage of wound healing and how to improve them is very active, with particular interest in the development of materials to enhance various stages of the wound healing process. The military for example has a great interest in the development of improved hemostatic agents, since controlling blood loss during battlefield wounding continues to be a challenge (Alam et al.) Many new technologies designed for rapid blood clotting on the front line involve supplementing the wound with natural or synthetic clotting factors, or cauterizing agents (Clay, Grayson and Zierold; Ellis-Behnke et al.). Although cauterizing minerals like QuikClot™ are very fast and effective, they release a large amount of heat, posing a risk of burn and tissue damage to the patient or responder (Arnaud et al.) In parallel, military and civilian wound care communities have pursued the use of new material solutions for improved cell proliferation beyond the hemostasis stage, such as the control of cellular growth and differentiation using bio-degradable silk fibroin scaffolds (Gupta et al.; Zhang, Baughman and Kaplan). Modification of silk fibroin films with inorganic clay materials has shown increased mechanical properties while maintaining biocompatibility (Kharlampieva et al.). Charged clay materials have been known for years to activate clotting factors, and certain layered clay species have demonstrated induction of coagulation at clotting times comparable to QuickClot™ without the release of heat (Baker et al.). Wound care specialists

focusing on the proper restoration of the skin's function after wounding are developing new epithelialization technologies such as skin grafts and improved vascularization (Simman, Craft and McKinney). Plastic surgeons are making advances in tissue remodeling techniques and topical applications to reduce scarring and improve the long term aesthetics of tissue remodeling following wound healing (van den Helder and Hage). Overall, modern research has gained much ground in producing technologies to advances individual stages of the wound healing process.

Herein we propose the hypothesis that clay-immobilized growth factor will effectively activate pro-growth cellular signaling for wound healing applications, which we have tested with three specific aims. First we study the intercalation efficiency and enzyme activity of HRP immobilized onto the surface of three aluminosilicate clays: MMT, kaolin, and halloysite. These clays each have certain features that make them suitable options for biomedical uses as described above. Second, we further select the clay with high binding efficiencies and enzyme activity, as well as a safe dosage of clay that produces no significant cell death *in vitro,* leading us to focus on the layered aluminosilicate clay MMT as a delivery mechanism for EGF. Third, we verify the functionality of EGF immobilized on Na-MMT by focusing on the activation of the AKT and mitogen activated protein kinase (MEK1) mediated pathways and their downstream effector molecules. We further confirmed that the spontaneously transformed keratinocyte cell line HaCaT, when treated with MMT-EGF, showed

increased migratory response dependent on activation of ERK1/2, a similar response to that of cells treated with EGF alone**.**

II. Materials and Methods

A. Materials.

Cloisite Na^+ (92.6 meq/100 g), a refined and purified naturally occurring sodium montmorillonite (Na-MMT), was purchased from Southern Clay Products, Inc. (Gonzales, TX). Kaolin and Halloysite nanoclay were purchased from Aldrich (St. Louis, MO). Horseradish peroxidase (HRP) was purchased as a lyophilized powder from Sigma (St. Louis, MO) and reconstituted at 5 mg/ml in 100 mM monopotassium phosphate buffer at pH 7. Glucose oxidase (GOX) was purchased as a lyophilized powder from Sigma and reconstituted at 1 mg/ml in 100 mM sodium acetate. 2,2'-Azino-bis(3-ethylbenzothiazoline-6-sulfonic acid) diammonium salt (ABTS) was purchased as a lyophilized powder from Sigma and reconstituted in dH_2O at pH 7 for immediate use. Human Recombinant Epidermal Growth Factor (hr-EGF) was purchased as a lyophilized powder from R&D Systems Inc. (Minneapolis, MN) and reconstituted at 100 µg/ml in 10 mM acetic acid. PD98059 (MEK1 inhibitor) was purchased from Cell Signaling Technologies (Beverly, MA) as a lyophilized powder and reconstituted at 20 mM in DMSO. Rapamycin (mTor inhibitor) was purchased from Calbiochem (San Diego, CA) and reconstituted at 10 mM in Ethanol.

B. Cell Culture.

Human spontaneously transformed keratinocyte cell line HaCaT was generously provided by Dr. Dori Germolec from the National Institute of

Environmental Health Sciences and were maintained in Dulbecco's modified Eagle's medium (DMEM) with 8 % fetal bovine calf serum (FBS) and 100 U penicillin and 100 µg streptomycin (1 % PS). Human primary fibroblast cell line IMR-90 was obtained from American Type Culture Collection (Manassas, VA), and were maintained in DMEM with 8 % FBS and 1 % PS.

C. Preparation of enzyme-clay nano complexes via solution mixing.

MMT, kaolin, or halloysite was added to de-ionized H_2O (dH_2O, pH 7) at a concentration of 10 mg/mL (1 % w/v) and vigorously stirred at room temperature for 48 hr with a magnetic stir bar, with MMT resulting in a yellow suspension and kaolin or halloysite resulting in a milky white suspension, which was autoclaved and stored at room temperature. Clay (1 mg) was washed with 1 mL of dH_2O (pH 7) and re-suspended in a total volume of 100 mL dH_2O. Reconstituted HRP (0.23 mg) was added to 15, 30, and 45 µl of the MMT, kaolin, or halloysite suspension, and the sample was brought up to a total volume of 1 mL of dH_2O. The samples were rotated overnight at 4 ˚C, washed 5X with phosphate buffer (pH 7), and re-suspended in 100 µl dH_2O. The supernatants were collected for immunoblot assay, and the clay-HRP suspension was used immediately for all experiments. Reconstituted GOX (1 mg) was added to 45 µl of the MMT suspension, then rotated overnight, washed 5 X with dH_2O, and prepared for X-ray diffraction characterization as described below.

D. Preparation of MMT-EGF nano complexes via solution mixing.

MMT (1 mg) was washed twice by manually re-suspending with 1 ml of dH_2O, pelleting, and discarding the supernatant, and the final pellet was re-suspended in a total volume of 100 µL dH_2O. EGF was bound to MMT by adding 50, 100, 250, or 500 ng of EGF, reconstituted in acetic acid, to 10 µl of the MMT suspension, and the sample was brought up to a total volume of 1 mL with dH_2O. The samples were rotated for 12 hr at 4 ˚C, washed 2X with dH_2O, and re-suspended in 100 µL dH_2O. The supernatants were collected to assay for EGF using immunoblot analysis, and the EGF-MMT suspension was used immediately for all experiments. For EGF desorption studies, 250 ng of reconstituted EGF was added to 10 µl of the MMT suspension, and the sample was brought up to a total volume of 1 ml culture media. The suspension was incubated at 37 ˚C and 5 % CO_2 for 72 hr. At 24 hr time points, the samples were pelleted and washed 2X with dH_2O, and the pellet and supernatant were collected for immuboblot assay.

E. Characterization of composite nano complexes.

MMT and MMT-enzyme samples were air-dried at room temperature onto glass coverslips into a powder and characterized by transmission X-ray diffraction (XRD). MMT and MMT-EGF nano complexes were lyophilized into a powder and characterized by XRD. A Rigaku rotating anode source (Cu-Kα), Statton camera and imaging plate detectors were used for data collection. X-Rays with a wavelength of 1.54 Å were used at distances of 53 mm and 175 mm

from the sample and data obtained was analyzed using the Fit2D software package (Andrew Hammersly, European Synchrotron Radiation Facility, Grenoble, France). A schematic of the experimental setup and associated values is depicted in Figure 3. The layer spacing was calculated using Bragg's Law,

$$n\lambda = 2d \sin\theta$$

and plotted against the scattering angle 2θ or the scattering vector q which can be defined as

$$q = 4\pi\lambda^{-1} \sin\left(\theta/_2\right)$$

with λ being the wavelength of the incident X-ray beam (1.54 Å), θ being the Bragg's scattering angle, d being the spacing between clay sheets, and n being an integer (in this case n = 1) (Ganguly, Bhowmick and Li). To analyze the surface topology and height of MMT and MMT-EGF, Atomic Force Microscopy (AFM) was performed using a Nanolink DPN 5000 Instrument equipped with a Pacific Nanotechnology closed-loop XYZ scanner. Pre-mounted close contact probes from Pacific Nanotechnology were used for imaging in close contact mode. The presence of EGF in MMT-EGF nano complexes was confirmed via immunoblot analysis as described below.

Figure 3. Schematic representation of x-ray diffraction characterization of layered clay. X-rays with a wavelength (λ) of 1.54 nm are diffracted off of the crystalline layers of the clay sample. The intensity of the diffraction is detected and plotted against the scattering angle 2θ. Using Bragg's equation, the interlayer spacing distance *d* can be calculated.

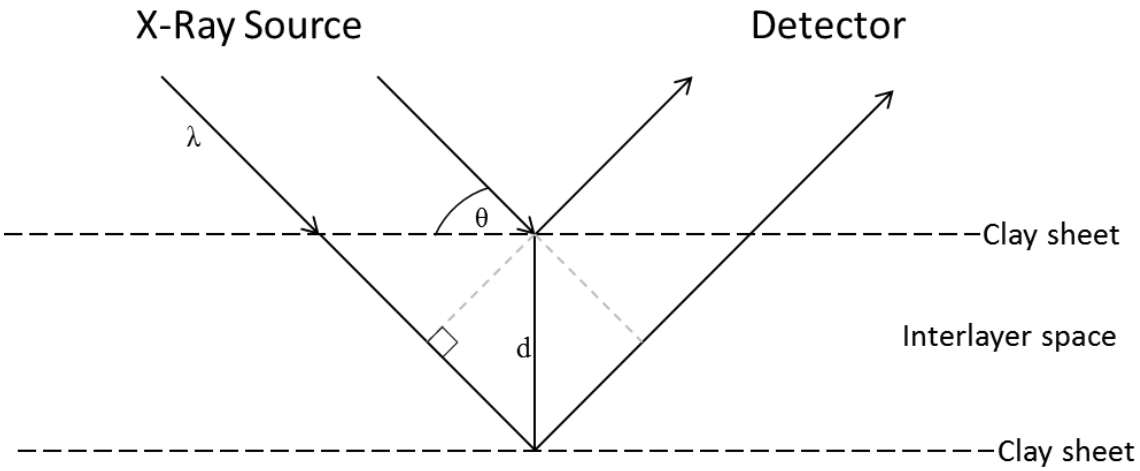
X-Ray Source
Detector
λ
θ
Clay sheet
Interlayer space
d
Clay sheet

F. Enzyme kinetics assay.

Reconstituted HRP (1 mg, pH 7) was added to 4.5 mg of MMT in a total volume of 1 ml dH_2O. The samples were rotated overnight at 4˚C and split into two 500 µl aliquots, then each was washed 5X with buffer of varying pH (4.5 or 7). The samples were reconstituted in 1 mL buffer of varying pH and rotated for 1 hr at 4 ˚C, then washed 3X and re-suspended in 1 ml buffer. Fractions (100 µl) of the final suspension were added to 100 µl ABTS of increasing concentrations and 30 µl of 0.003 % H_2O_2 in a 96-well plate, and the absorbance at 405 nm was measured at 11 second kinetic intervals using a Tecan Safire-2 plate reader and analyzed using the Magellan software package (Tecan). Reconstituted HRP (100 ng) was included under the same conditions as a positive control. The raw data was plotted as time (seconds) versus absorbance intensity for each substrate concentration (S), and the initial reaction velocity (V) was calculated from the slope using a linear fit trend line. The final results were analyzed using the SigmaPlot software package as a non-linear regression of the plot of V versus S.

G. Cell proliferation assay.

Cells were plated at a density of 2.5×10^5 cells/well (HaCaT) or 5×10^4 cells/well (IMR-90) in a six-well plate, and incubated at 37 ˚C and 5 % CO_2. MMT (1 % w/v) diluted to 0.1 %, 0.05%, 0.01 %, and 0.001 % in dH_2O in a total volume of 2 ml was washed 2X with dH_2O and 2X with DMEM, and resuspended in 2 ml of fresh DMEM. At 24 hr post-plating of cells, the normal culture media was replaced with complete DMEM containing MMT of the aforementioned

concentrations. Cells were harvested at 0, 24 and 48 hr post-treatment, stained with trypan blue and manually counted. A separate culture well was used for each time point measurement. The 0 hr time point contained no MMT, and was used to establish a baseline plating density for all conditions.

H. Bright field and immunoflorescent imaging of IMR-90 cells post-MMT treatment.

For bright field imaging, IMR-90 cells were plated at a density of 5×10^5 cells/well in a six-well plate. At 24 hr after seeding, cells were treated with increasing concentrations of MMT for 24 hr, then washed 3X with sterile PBS and imaged using a Leica DMI-6000B microscope. For immunofluorescence staining, IMR-90 cells were plated on sterilized coverslips at a density of 5×10^5 cells/well in a six-well plate. Cells were fixed with 2 % paraformaldehyde for 15 min followed by permeabilization with 0.2 % Triton X-100 for 5 min. Cells were blocked with 0.5 % normal goat serum (NGS) and incubated with primary antibody against α-tubulin (1:4,000 dilution) for 1hr at room temperature. After three washes with 0.5 % NGS, cells were incubated with secondary goat anti-mouse, Texas-red conjugated antibody (1:500 dilution) (Jackson Immunoresearch, West Grove, PA). VectaShield DAPI-containing fixing solution was used for nuclear staining. A Leica DMI-6000B microscope was used for imaging of the samples.

I. Confocal immunofluorescence analysis of EGFR activation.

HaCaT cells were plated on sterilized glass coverslips at a density of 2.5 × 10^5 cells/well in a six-well plate. At 24 hr after seeding, cells were serum starved for 24 hr followed by treatment with EGF or MMT-EGF for 30 min. For immunofluorescence staining, cells were fixed with 2 % paraformaldehyde for 15 min followed by permeabilization with 0.2 % Triton X-100 for 5 min. Cells were blocked with 0.5 % normal goat serum (NGS) and incubated with primary antibody against phospho-EGFR (1:1500 dilution) for 1 hr at room temperature. After three washes with 0.5 % NGS, cells were incubated with secondary goat anti-rabbit, fluorescein isothiocyanate (FITC)-conjugated antibody (1:500 dilution) (Invitrogen, Carlsbad, CA). VectaShield DAPI-containing fixing solution was used for nuclear staining. A Zeiss LSM-700 microscope was used for confocal imaging of the samples (Carl Zeiss MicroImaging, LLC, Thornwood, NY).

J. Western blot analysis.

HRP immobilization on MMT, kaolin, and halloysite was confirmed by fractioning clay pellets or supernatants onto a 7 % SDS polyacrylamide gel electrophoresis (PAGE). Densitometry analysis was conducted using the Multigauge software package (Fuji). EGF immobilization on MMT was confirmed by fractionating clay pellets or supernatant onto a 15 % SDS polyacrylamide gel. HaCaT cells treated with EGF or MMT-EGF in presence or absence of pre-treatment with PD98059 (MEK1 inhibitor) or Rapamycin (mTOR inhibitor) were harvested and whole cell extracts were prepared by lysing the cells in

phosphatase inhibitors containing buffer (50 mM Tris-HCl pH 8, 120 mM NaCl, 5 mM NaPPi, 10 mM NaF, 30 mM paranitrophenylphosphate, 1 mM benzamidine, 0.1 % NP-40, 1 % Triton X-100 and 0.2 mM PMSF, 100 nM sodium orthovanadate) supplemented with protease inhibitors. Equivalent amount of these whole cell extracts were run on a 10 % SDS PAGE. Samples were then transferred to a PVDF membrane and the membrane was blocked using 1 % BSA in tris-tween buffered saline (TTBS) for phosophorylated proteins or 5 % nonfat milk in TTBS for non-phosphorylated proteins. Membranes were then probed with antibodies overnight at 4 °C that were specific for HRP (Abcam, Cambridge, MA), EGF (Sigma, St Louis, MO), total and phosphorylated AKT, GSK3β, S6, and ERK (Cell Signaling Technologies, Danvers, MA), phosphorylated EGFR (Cell Signaling Technologies), and finally β-actin (Sigma, St Louis, MO) which was used as a loading control. Appropriate secondary HRP-conjugated antibodies for immunoblotting were obtained from Promega (Madison, WI), and used to probe the membranes for 1 hr at room temperature. The membranes were developed using chemiluminescence as previously described (Kommagani et al.).

K. Wound closure assay.

In vitro scratch-wound closure assay was used to measure the migration of cells after treatment with EGF-MMT (Zeineldin and Hudson). Cells were plated at a density of 4 x 10^5 cells/well (HaCaT) or 5 x 10^5 cells/well (IMR-90) in a six-well plate and cultured in complete DMEM to near confluence. The cells were then serum starved for 24 hr following which each well was manually

scratched with a micro-pipet to create two parallel vertical scratches and one perpendicular horizontal scratch, creating two intersections used as points of reference, and washed 3X with sterile PBS to remove cell debris. The cells were then treated with EGF, MMT, or EGF-MMT equilibrated in serum-free DMEM were added at a concentration of 5 ng/mL EGF (growth factor concentration in EGF-MMT was estimated based on the loading conditions of 25 ng EGF/1 µg MMT). Percentage of wound closure after *t* hours was observed by bright-field microscopy at 100X magnification, and quantified using the formula

$$\left(\frac{wound\ area_{t0} - wound\ area_{t1}}{wound\ area_{t0}}\right) \times 100$$

Images were taken at the vertical portions of the two scratch intersections yielding four total frames. Reported data are the averages and standard deviations from at least three frames during a single representative experiment. The experiment was repeated 3 times yielding similar trends. The scratch-wound assay was repeated using HaCaTs with an additional 4 hr pre-treatment with rapamycin (RAPA) or PD98059 inhibitors prior to treatment with EGF or EGF-MMT. A control sample was pre-treated for 5 hr with DMSO vehicle.

L. Quantitative real-time polymerase chain reaction (qRT-PCR) analysis.

HaCaT cells were plated at a density of 2.5×10^5 cells/well in a six well plate. After 24 hr of seeding, the cells were serum starved for 24 hr, pretreated for 2 hr with 100 nM RAPA or 75 µM PD98059 followed by treatment with serum free DMEM supplemented with 5 ng/mL EGF or 0.001 % MMT-EGF. At 1 hr post-treatment total RNA from cells was extracted using eZNA RNA isolation kit

(Omega Bio-tex, Norcross, GA) according to manufacturer's protocol. A total of 1 µg RNA was used to synthesize cDNA by using TaqMan reverse transcription kit (Applied Biosystems, Foster City, CA). TaqMan based real-time PCR analysis was performed in a 96 well microtiter plate format on an ABI Prism7900HT sequence detection system using TaqMan 2X master mix and gene specific assays on demand, and normalized to endogenous GAPDH endogenous control (part # 4326317E) (PE Applied Biosystems, Foster City, CA). Assays on demand (AOD) were used for S100A2 (Hs_00195582_m1), VEGF (Hs_00900054_m1), and THBS1 (Hs_00170236_m1) (Applied Biosystems, Foster City, CA). Relative mRNA quantitation was performed using the comparative $\Delta\Delta$Ct method (Pfaffl).

III. Results.

A. Characterization of clay-enzyme complexes.

Immunoblot analysis (western blot) is a commonly used technique to identify and quantify proteins based on antibody affinity for a specific amino acid sequence (Burnette). Here, we used immunoblot analysis to confirm immobilization of HRP to the clay surface and measure the binding capacity to MMT, kaolin, or halloysite via comparative densitometry of the resulting bands. To prepare the clay-HRP samples for analysis, 15, 30, and 45 µl of 1 wt % MMT, kaolin, or halloysite were incubated with 0.23 mg HRP in a final volume of 1 ml in dH2O, and rotated overnight at 4 ˚C. The clay was pelleted, and fractions of the pellet were subject to immunoblot analysis using HRP-specific antibodies. As shown in Figure 4A**,** we demonstrated binding of HRP to MMT only, with little to no binding to kaolin and halloysite. This is expected due to the strong surface charge and ion exchange capacity of Na-MMT (Lozzi et al.). To quantitate the amount of HRP bound to MMT surface, we compared the band intensity of the MMT-HRP fractions containing unknown amounts of HRP, to a series of known HRP concentrations. As seen in Figure 4B, a concentration dependent increase in HRP binding is observed in the MMT pellet with increasing concentrations of MMT. By comparing the densities of unknown HRP concentrations in the pellet to the standard curve, we can calculate the binding capacity to be 0.070 (± 0.006) ng of HRP per 1 µg MMT. This value was used to estimate the amount of HRP enzyme in our MMT-HRP pellet for future studies such as enzyme kinetics.

Figure 4. Western blot analysis of clay-horseradish peroxidase nanocomposites. A. Immunoblot analysis of increasing amounts of MMT, kaolin (K), or Halloysite (H) incubated with an excess of HRP. Pellet fractions were resolved on a 10 % SDS-PAGE and probed with anti-HRP. HRP standards were also subject to immunoblot analysis. B. Density of the MMT-HRP pellet was plotted against a linearly fit HRP standard curve.

A.

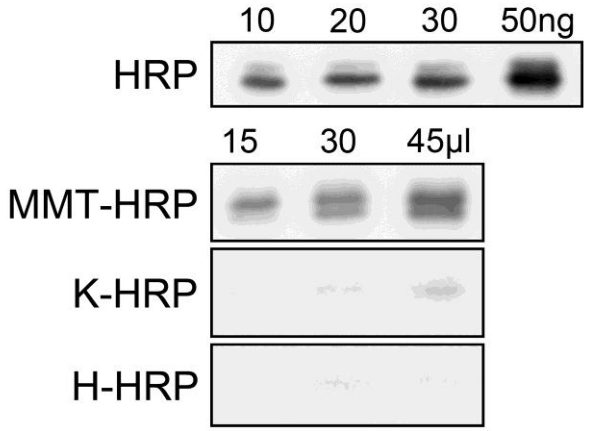
10
20
30
50ng
HRP
15
30
45µl
MMT-HRP
K-HRP
H-HRP

B.

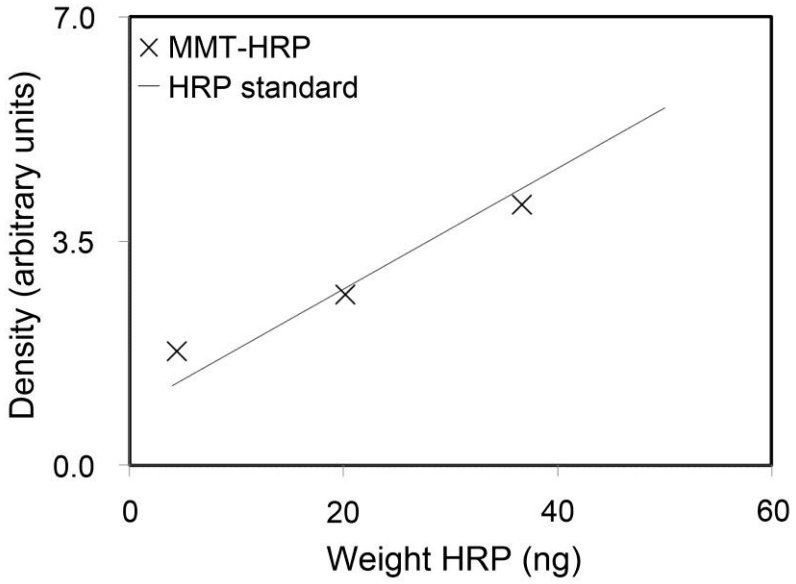
7.0
3.5
0.0
MMT-HRP
HRP standard
Density (arbitrary units)
0
20
40
60
Weight HRP (ng)

MMT-HRP was further characterized by powder x-ray diffraction (XRD), a technique commonly used to analyze the change in lattice spacing of layered materials such as clay sheets occurring as a result of intercalation with different molecular species (Sanjay and Sugunan). A second enzyme glucose oxidase (GOX), known to intercalate into Na-MMT, was also examined for comparison (Garwood, Mortland and Pinnavaia). MMT (45 µl of 0.1 % w/v) was incubated with a solution of HRP or GOX as previously described. Fractions of the sample were dried into a powder and subject to XRD analysis. The diffraction intensity plotted against the scattering vector *q* in Figure 5 shows a shift in the peak representing basal layer spacing due to intercalation of HRP or GOX. The structure of recombinant HRP has been determined by XRD to measure approximately 5 nm x 3.7 nm, corresponding to an estimated increase in layer spacing of 3 nm as indicated by Figure 5 after accounting for dehydration and sample preparation (Berglund et al.). It can be hypothesized from this that the globular structure of HRP is conserved as it binds to MMT. In contrast, the structure GOX is known through crystallography to measure approximately 6.7 nm x 4.8 nm, while the diffraction pattern of MMT-GOX instead reflects a spacing change of 0.8 nm and 3.9 nm. This is likely due to denaturation of GOX upon intercalation within MMT sheets which has been previously observed (Garwood, Mortland and Pinnavaia).

Figure 5. X-ray diffraction characterization of enzyme bound MMT.

Powder XRD of air dried Na-MMT complexes. An increase in peaks representing basal layer spacing is observed from 1.0 nm in MMT only (black) to 4.0 nm with the addition of horseradish peroxidase (MMT-HRP, red), and 1.8 nm and 4.9 nm with the addition of glucose oxidase (MMT-GOX, blue) due to intercalation of enzyme within the layers of stacked MMT.

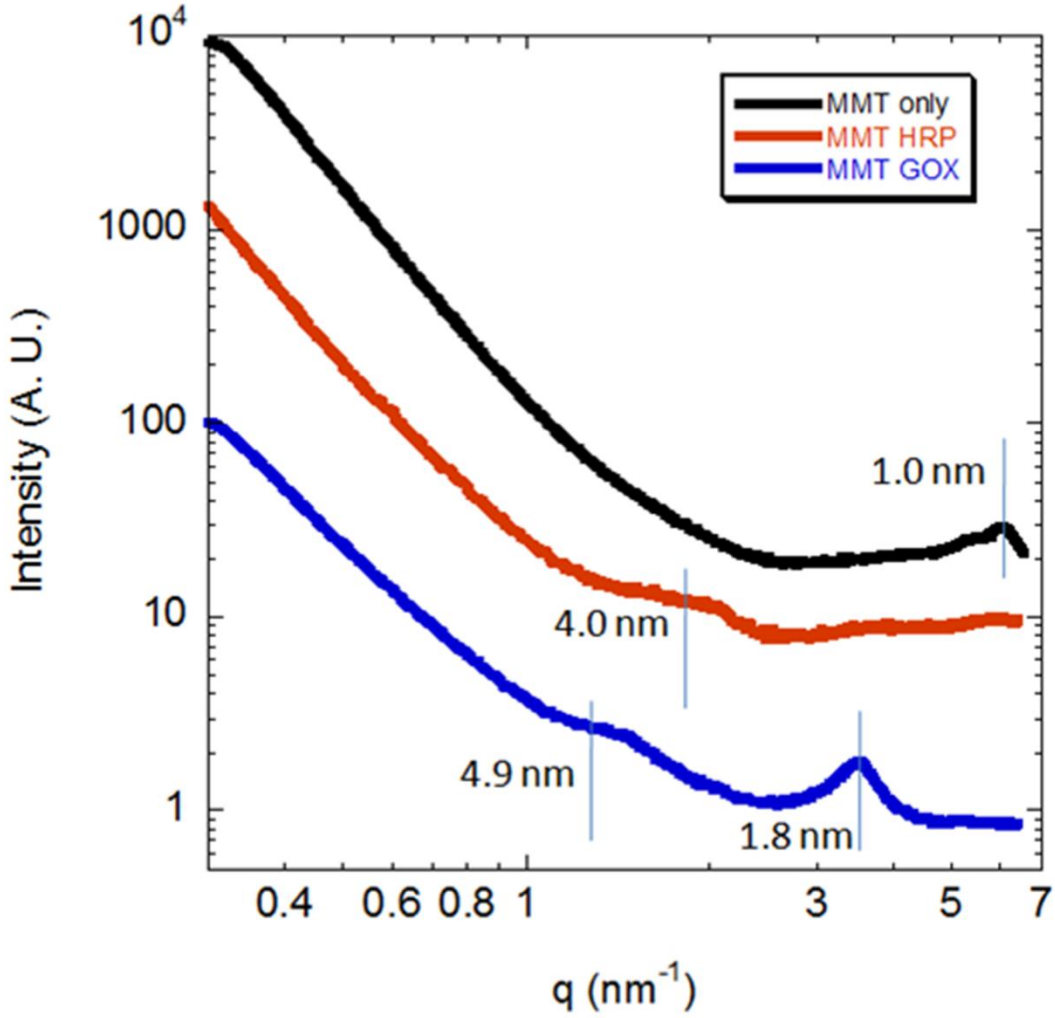
MMT only
MMT HRP
MMT GOX
1.0 nm
4.0 nm
4.9 nm
1.8 nm
Intensity (A. U.)
q (nm-1)
10^4
1000
100
10
1
0.4
0.6
0.8
1
3
5
7

B. MMT-HRP exhibits stabilized Michaelis-Menten kinetics.

When analyzing activity of enzymes, kinetic values will give a detailed account of the reaction between an enzyme and its substrate. As an enzyme population [E] binds with a substrate [S] it will form an intermediate complex [ES], which will form and break apart at equilibrium (at a rate of k_1 and k_{-1}). From the enzyme-substrate complex a product [P] is formed at a rate of k_2, and the enzyme returns to its previous state [E]. This can be summed by the following relationship:

$$[E] + [S] \underset{k_1}{\overset{k_{-1}}{\longleftrightarrow}} [ES] \underset{k_2}{\rightarrow} [E] + [P]$$

The Michaelis-Menten kinetic parameter, K_m, can be loosely defined as the ratio of the rate of dissociation to association of the enzyme-substrate complex, and is mathematically defined as:

$$K_m = \frac{k_{-1} + k_2}{k_1}$$

Other kinetic parameters include V_{max} which indicates the maximum velocity at which product formation will occur, and k_{cat} which indicates the turnover rate of product formation, and are related through the following:

$$V_{max} \overset{\text{def}}{=} k_{cat} \times E_{total}$$

where E_{total} represents the total amount of enzyme (Michaelis and Menten). Kinetic values can be determined through a non-linearly fit curve as a result of the initial reaction velocity V_i versus substrate concentration [S] (Jones). It is also

possible to graphically visualize the kinetic data using an extrapolation of one of several linear regressions, namely the Linweaver-Burke plot, Eadie-Hofstie plot, or the Hanes-Woolfe plot.

Although the globular structure of HRP appears to be conserved when bound to MMT, there are many factors that will affect enzyme activity when bound versus free in solution. Some studies have shown a decrease in activity of immobilized enzymes, while others show stabilization of activity due to molecular crowding (Lozzi et al.; Dunker and Fernandez). We compared the enzyme activity of 100 ng of free versus MMT-immobilized HRP (enzyme concentration in MMT-HRP was estimated based on calculations as previously described). Experiments were done in 100 mM monopotassium phosphate buffer at pH 9 and pH 4 using ABTS as a substrate for HRP. The initial reaction velocity (V_i) of free and immobilized HRP reacted with H_2O_2 and increasing concentrations of ABTS substrate (S) is plotted in Figure 6 as a V versus S plot, and in Figure 7 as a Lineweaver-Burk plot, and all conditions result in a Michaelis-Menten kinetic profile. While the activity of free HRP in solution is diminished at pH 4.5, the activity of MMT-HRP is stabilized to an extent which may occur through physical stabilization of the enzyme and protection from the harsh acidic environment, or through a buffering effect due to the inherent charged properties of MMT. The associated kinetic (V_{max}, K_m, and K_{cat}) values were derived from the non-linear regression of the V vs S plot and are shown in Table 1. From this data we can conclude that HRP immobilized on the surface of MMT in aqueous suspension will retain biological activity, and that the MMT itself

may act to protect the enzyme from the environment. Using this system as a model, we predicted that EGF bound to MMT will also retain biological activity in an aqueous environment.

Figure 6. MMT-HRP exhibits stabilized Michaelis-Menten kinetics at varying pH. Free HRP and MMT-HRP kinetics upon reaction with ABTS substrate as described in materials and methods. V versus S plots of each condition indicate Michaelis-Menten kinetics with full activity at pH 7, while HRP-MMT activity remains stabilized at pH 4.5.

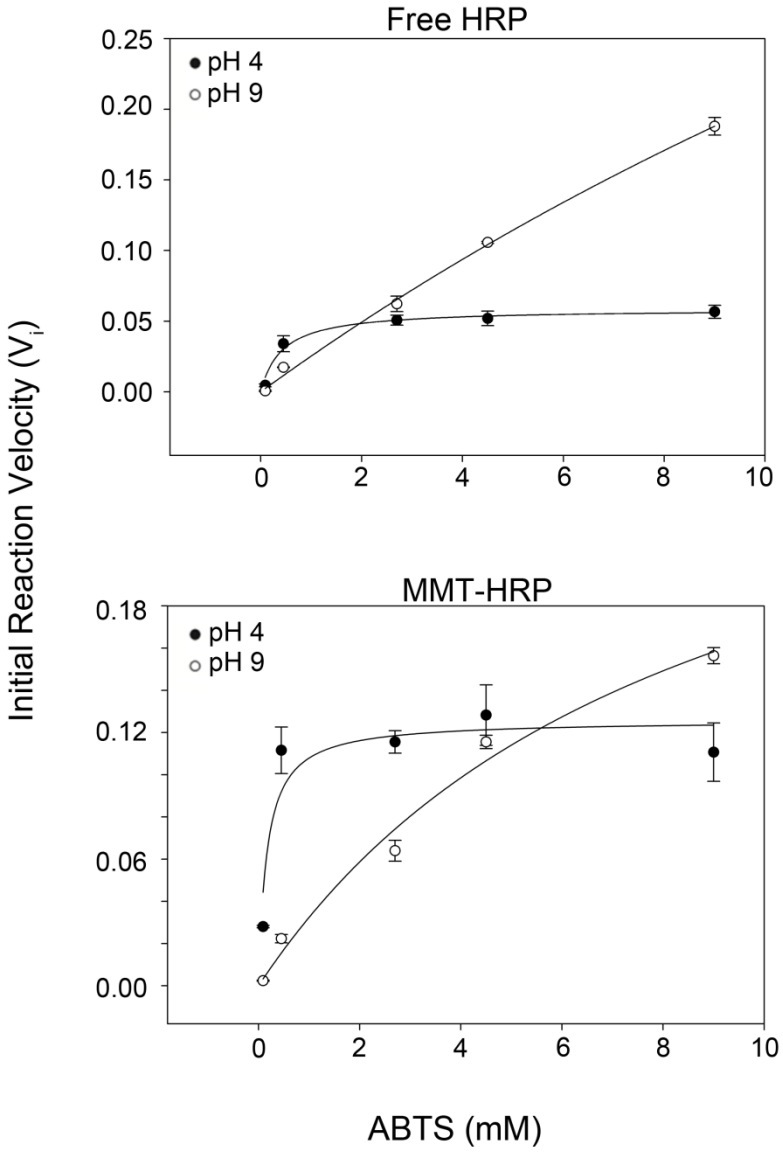
Free HRP
pH 4
pH 9
0.25
0.20
0.15
0.10
0.05
0.00
0
2
4
6
8
10
MMT-HRP
pH 4
pH 9
0.18
0.12
0.06
0.00
0
2
4
6
8
10
Initial Reaction Velocity (V$_i$)
ABTS (mM)

Figure 7. Lineweaver-Burke plot of the activity of free HRP versus MMT-HRP. The linear regression derived from the double reciprocal plot indicate a similar change in activity of free and MMT-bound HRP upon a shift in pH.

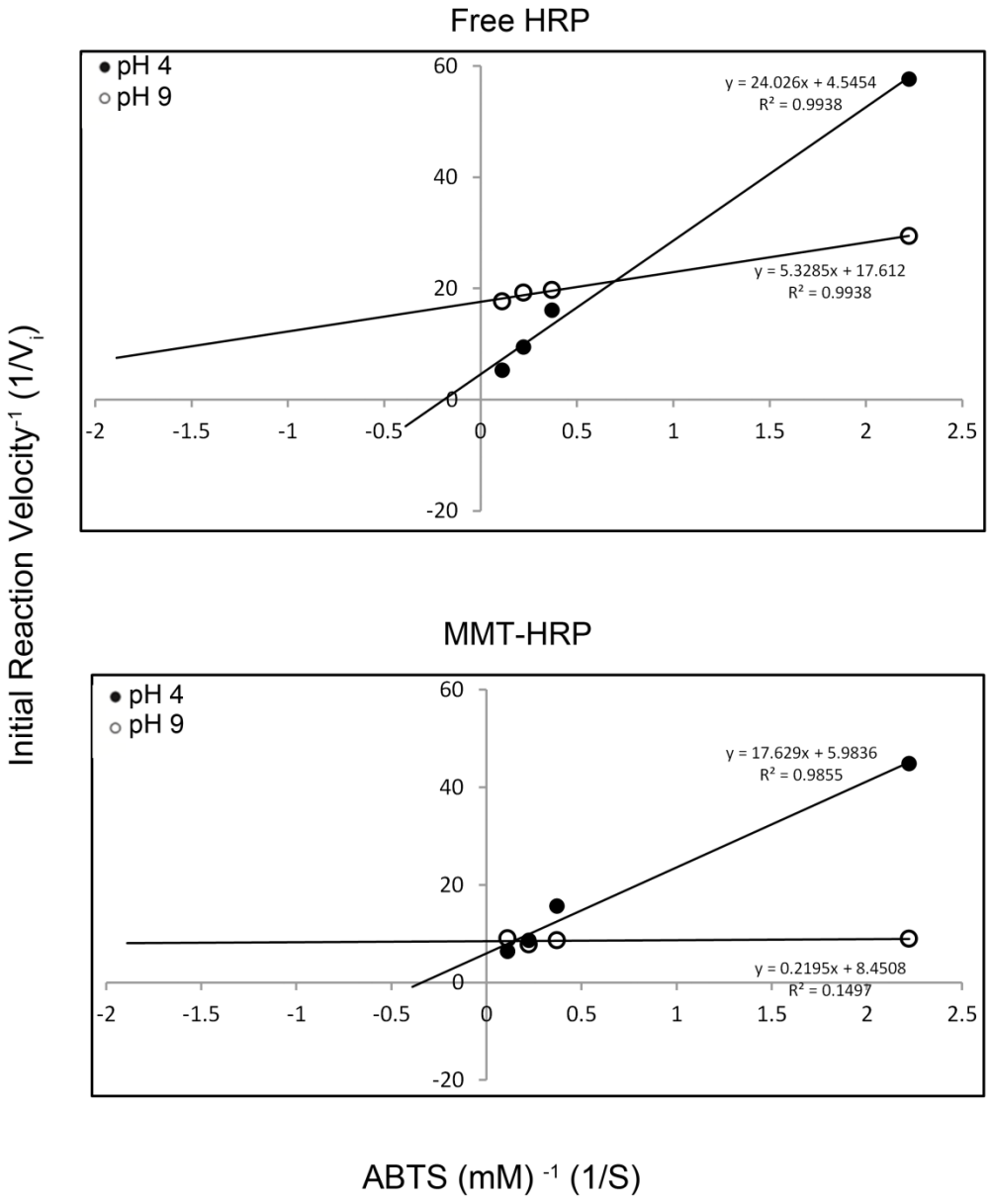
Free HRP
pH 4
pH 9
y = 24.026x + 4.5454
R² = 0.9938
y = 5.3285x + 17.612
R² = 0.9938
60
40
20
0
-20
-2
-1.5
-1
-0.5
0
0.5
1
1.5
2
2.5
MMT-HRP
pH 4
pH 9
y = 17.629x + 5.9836
R² = 0.9855
y = 0.2195x + 8.4508
R² = 0.1497
60
40
20
0
-20
-2
-1.5
-1
-0.5
0
0.5
1
1.5
2
2.5
Initial Reaction Velocity-1 (1/Vi)
ABTS (mM) -1 (1/S)

Table 1. Enzyme kinetic values of free and MMT-immobilized HRP at pH 7 and pH 4.5. Quantification of enzyme kinetic parameters based on the Linweaver-Burke plot in figure 7.

	K_m (mM)	V_{max} (mM)	k_{cat} (sec^{-1})
Free HRP pH 9	37.0	0.96	160.0
MMT-HRP pH 9	8.5	0.31	51.7
Free HRP pH 4	0.42	0.059	9.8
MMT-HRP pH 4	0.17	0.13	21.7

C. MMT, kaolin, and halloysite inhibit keratinocyte and fibroblast proliferation in a dose dependent manner.

To study the effect of MMT, kaolin, and halloysite on cell growth we cultured HaCaT cells in the presence of increasing concentration of MMT, kaolin, and halloysite. Since it can be assumed that some biomolecular species within the culture media may bind to MMT, clay samples were pre-incubated in culture media, pelleted, and then added to the cells in a suspension of fresh media to mitigate the further removal of essential growth nutrients. Cell growth was monitored for up to 48 hrs post-treatment using trypan-blue staining every 24 hrs. As shown in Figure 8**,** reduction in cell viability of HaCaT cells was observed when clay concentration exceeded 0.01 % in all cases. A similar dose-dependent decrease in cell viability has been observed in human hepatoma HepG2 cells upon exposure to Na-MMT, with clay treatments in excess of 50 µg/ml (0.005 % w/v) inducing cell membrane damage due to reactive oxygen species generation (Lordan, Kennedy and Higginbotham; Dunker and Fernández). However, HaCaT cells exhibit resilience at MMT concentration of 0.001 %, resulting in no significant decrease in cell growth. Therefore subsequent experiments were performed using 0.001 % MMT. Since MMT was shown to have the best binding capacity to biomolecules such as HRP and GOX, MMT was used in all further experiments.

Figure 8. Dose dependent survival of HaCaT and IMR-90 cells upon treatment with increasing clay concentrations. HaCaT cells ($2.5x10^5$) or IMR-90 cells ($5x10^4$) were seeded in 6-well plates. After 24 hr the media was replaced with DMEM containing increasing concentrations of MMT, halloysite (H), or kaolin (K). Cells were harvested by trypsinization, subjected to live-dead staining with trypan blue, and manually counted on a hemocytometer. Cells were counted before clay addition (0 hr), and at 24 and 48 hr post-treatment. The y-axis represents the total number of cells. Data shown is the average of three independent experiments.

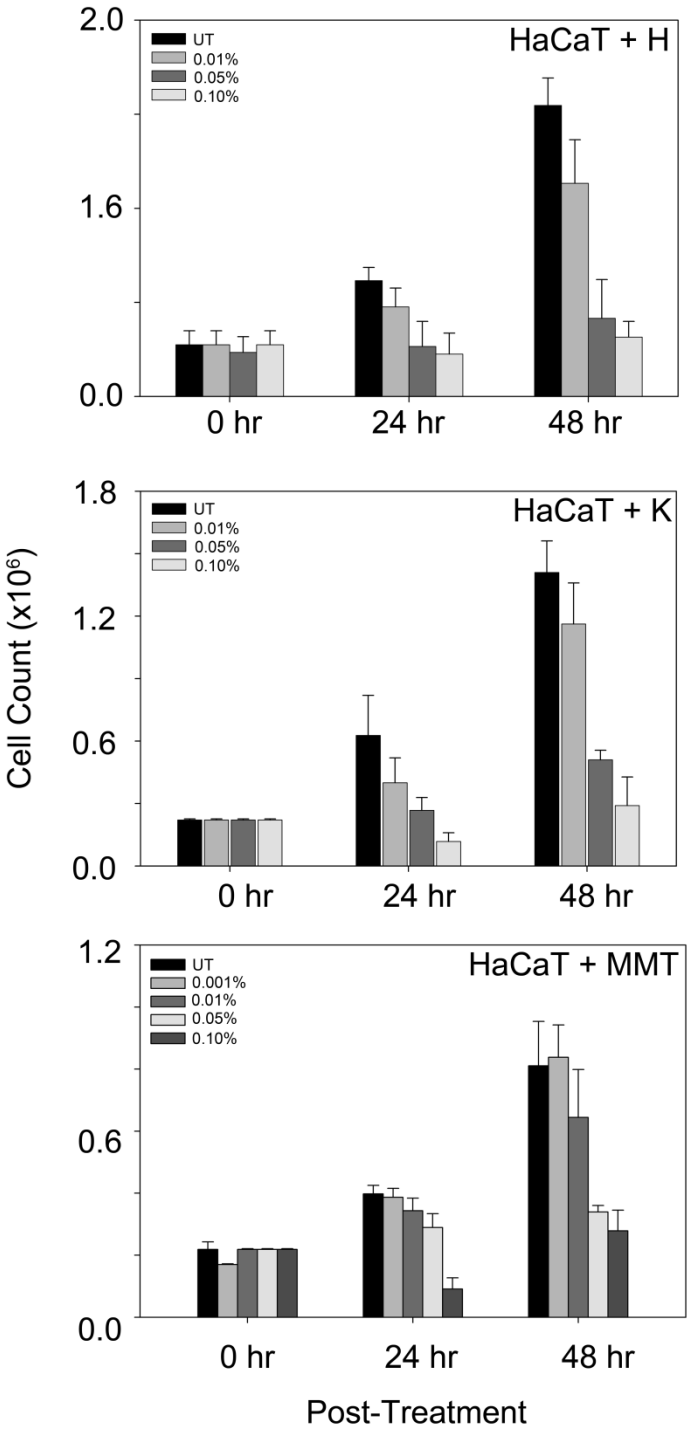
HaCaT + H
UT
0.01%
0.05%
0.10%
2.0
1.6
0.0
0 hr
24 hr
48 hr
HaCaT + K
1.8
1.2
0.6
0.0
Cell Count (x10⁶)
HaCaT + MMT
UT
0.001%
0.01%
0.05%
0.10%
1.2
0.6
0.0
Post-Treatment

It is important to better understand the affect clay has on primary cells, which serve as a more accurate model of the *in vivo* system. To do this, we cultured IMR-90 fibroblast cells in the presence of increasing concentrations of MMT. An approximate 50 % reduction in cell viability with as little as 0.01 % MMT treatment was observed in IMR-90 cells as shown in Figure 9. The sensitivity of IMR-90 cells to clays can be attributed in part to their primary nature. When observed visually, MMT particles can be seen to aggregate and adhere to the cell surface. Figure 10A shows bright field images of IMR-90 cells untreated or treated with increasing doses of MMT. Aggregates of MMT can be seen in contact with the cell membrane at MMT concentrations of 0.01 % and 0.05 %, and a coating of MMT on the cells and surrounding areas of the culture dish can be seen at a concentration of 0.1 %. As aggregation occurs on the cell surface with increasing concentrations of MMT, the cells can be shown to clump and cell movement can be inhibited as shown by immunofluorescent images in Figure 10B. While untreated IMR90 cells (UT) exhibit extended, out-stretched morphologies, cells treated with MMT began to stick together and were inhibited from cell spreading. Although clay adhesion to cell membranes *in vitro* exhibits such negative effects on proliferation and morphology at high concentrations, this property may be beneficial at lower concentrations in applications such as epidermal growth factor delivery. Areas of wound healing during injury are very congested with biomolecules, including platelets, macrophages, enzymes, clotting factors, and many other molecules entering and exiting the area.

Figure 9. Dose dependent survival of IMR-90 cells upon treatment with increasing clay concentrations. IMR-90 cells ($5x10^4$) were seeded in 6-well plates, and treated with MMT as described above.

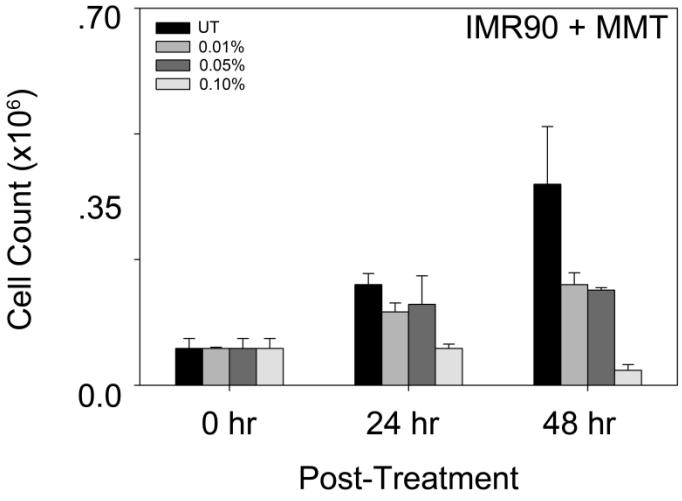
IMR90 + MMT
UT
0.01%
0.05%
0.10%
Cell Count (x10^6)
.70
.35
0.0
0 hr
24 hr
48 hr
Post-Treatment

Figure 10. MMT clay particles adhere to the surface of IMR-90 cells and cause aggregation. A. IMR-90 cells were plated in a six-well plate and at 24 hr after seeding cells were treated with normal media, or media containing .01%, .05%, or 0.1% MMT for 24 hr. Cells were washed 5X with sterile PBS, and imaged with bright field microscopy. B. IMR-90 cells were plated on sterilized coverslips in a six-well plate. At 24 hr after seeding, cells were treated with media containing MMT for 24 hr before fixing and staining. Cells were fixed and stained for α-tubulin (botom) and DAPI was used to stain the nuclei (top) and imaged using fluorescence microscopy.

A.

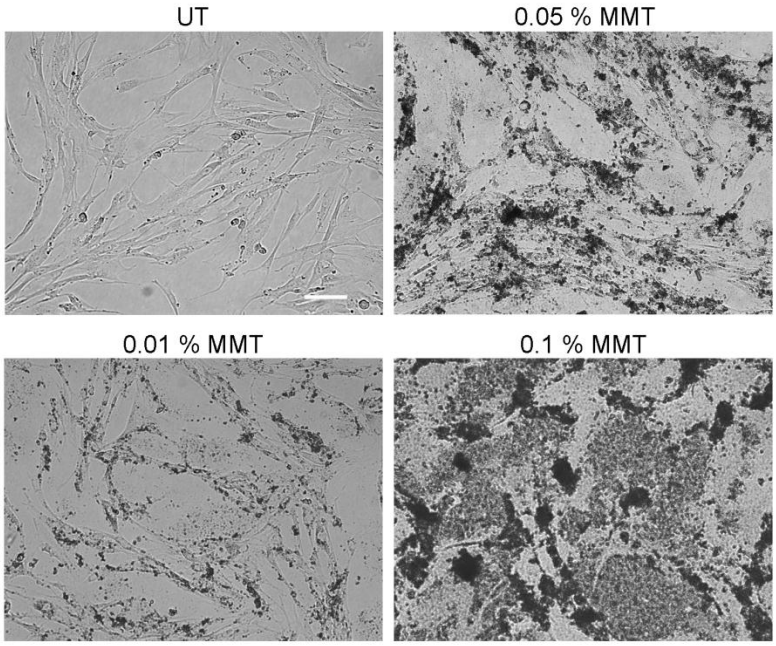

B.

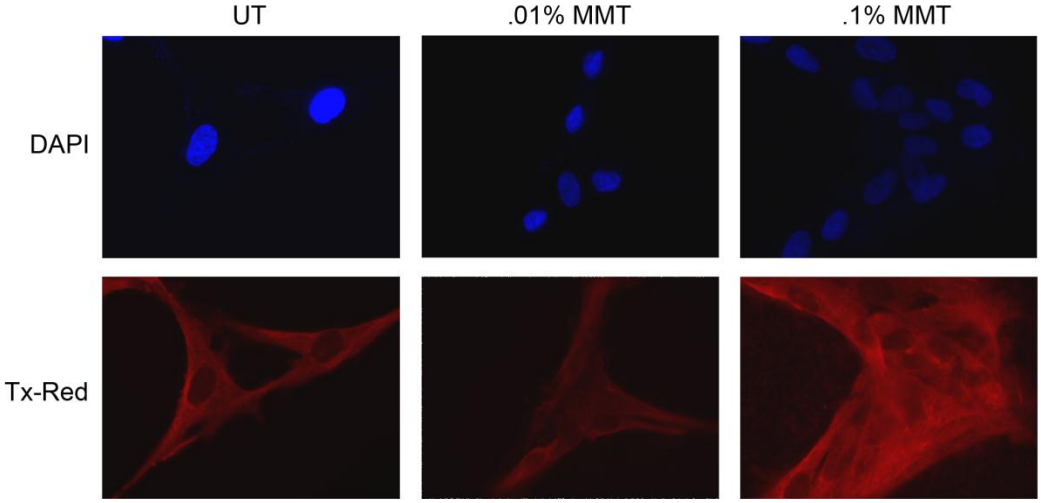

Adhesion directly to the cell membrane by MMT-EGF may prove advantageous for efficient delivery of growth factor to the healing cells.

D. Characterization of MMT-EGF complexes.

Since the previously described MMT-HRP model system suggested to us that MMT is a viable candidate clay for the delivery of EGF, we next sought to repeat the experimental procedures using EGF as the exchangeable biomolecule. Immunoblot analysis of MMT-EGF nanocomposite and supernatant using EGF-specific antibodies was used to confirm the binding of MMT to EGF. A 10 µl aliquot of 1 wt % MMT suspension (100 µg MMT) incubated with 50, 100, 250, or 500 ng of reconstituted EGF in a final volume of 1 mL in dH_2O was rotated for 12 hr at 4 ˚C. The MMT was pelleted and supernatant was collected after rotation to measure un-bound EGF. As shown in Figure 11A, 1 mg MMT fully absorbs 250 ng EGF with maximum binding occurring between 250-500 ng, as unbound EGF was only detected in the supernatant when EGF was in excess of 250 ng. Since the cation exchange capacity (CEC) of Cloisite-Na® is known to be 92.6 meq/100g clay, a loading concentration of 250 ng EGF per 1 mg MMT can be calculated to occupy 0.12 % of the available ion exchange sites on the MMT surface. The remaining 99.9 % of the exchange sites continue to be occupied by Na^+, which should allow Na-MMT to retain the ability to induce cationic activation of clotting factors. From this data we selected a concentration of 250 ng EGF per 1 mg MMT for subsequent experiments.

Figure 11. Characterization of MMT-EGF nanocomplexes. A. Immunoblot analysis of clay pellets and supernatants from 1 mg MMT incubated with increasing concentrations of EGF using anti-EGF antibodies. The supernatant (sup) was collected to assay for un-bound EGF. EGF standards were also subject to immunoblot analysis as shown in the lower panel. B. Powder XRD of freeze-dried Na-MMT and MMT-EGF. The peak at $2\theta = 8.3$ (001) indicates a basal layer spacing of approximately 1.1 nm, with no significant change in stacking of MMT upon the addition of EGF.

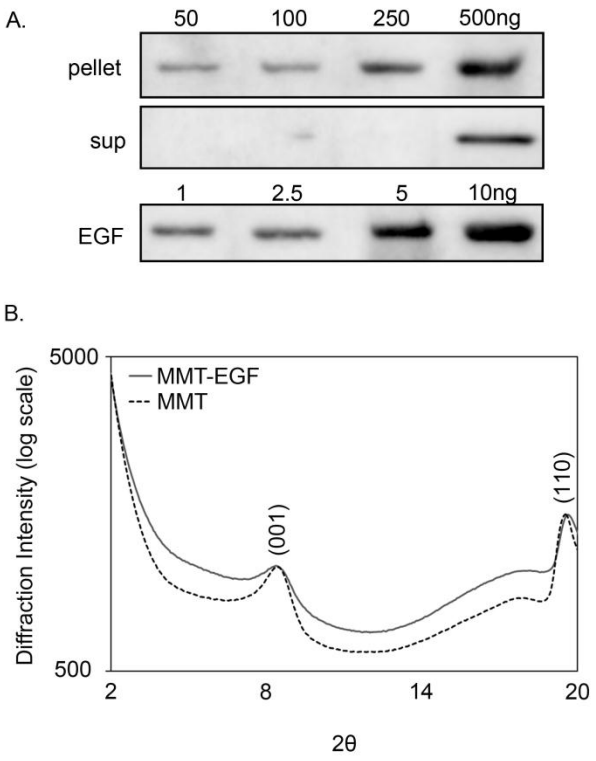
A.
50
100
250
500ng
pellet
sup
1
2.5
5
10ng
EGF
B.
5000
500
MMT-EGF
MMT
(001)
(110)
Diffraction Intensity (log scale)
2
8
14
20
2θ

MMT-EGF was further characterized by powder XRD. The diffraction intensity plotted against 2θ in Figure 11B resembles the typical diffraction pattern of Na-MMT. The prominent peak at 2θ = 8.3 represent a characteristic 1.06 nm repeat distance of bare MMT crystallite sheet stacking, and reflects an approximate monolayer of H_2O molecules hydrating the Na^+ cations within the gallery between the aluminosilicte layers. Unlike intercalation of some biomolecules within MMT such as HRP which cause a uniform change in inter-lattice spacing, addition of EGF to MMT does not lead to a distinct shift in repeat distance, indicating minimal to no intercalation (Lozzi et al.). AFM analysis demonstrates that the binding of EGF molecules to MMT causes little to no change in the crystallite structure of MMT as shown in Figure 12. A height increase of 1 nm can be seen in individual MMT sheets upon the addition of EGF and may be due to surface binding of EGF; however this has not been fully characterized.

To measure the stability of MMT-EGF in cell culture media we incubated MMT-EGF suspensions in complete culture media at 37 ˚C and 5 % CO_2 and analyzed the supernatant for EGF that had detached from the clay pellet up to 72 hrs. The starting materials are shown in Figure 13A with “media” representing the amount of EGF present in complete culture media itself, “10 ng EGF” as a reference point, and “MMT-EGF” as the amount of EGF in a fresh MMT-EGF pellet. As shown in Figure 13B, a sample of MMT-EGF incubated at 37 ˚C and 5 % CO_2 for 72 hr was pelleted every 24 hr to collect the supernatant for analysis of detached EGF. The MMT-EGF pellet was subject to immunoblot analysis for

Figure 12. AFM analysis of MMT-EGF nanocomplexes. Atomic force microscopy imaging of MMT (A-B) and MMT-EGF (D-E) with their corresponding height profiles (C and F). 10µl samples of MMT or MMT-EGF suspension were dried onto silicon wafers and imaged. A height profile measured between the blue and red arrows indicate an increase of approximately 1 nm when EGF is bound to the surface. Images displayed are representative of two independent experiments. AFM experimentation and data analysis was carried out by Kristi Singh.

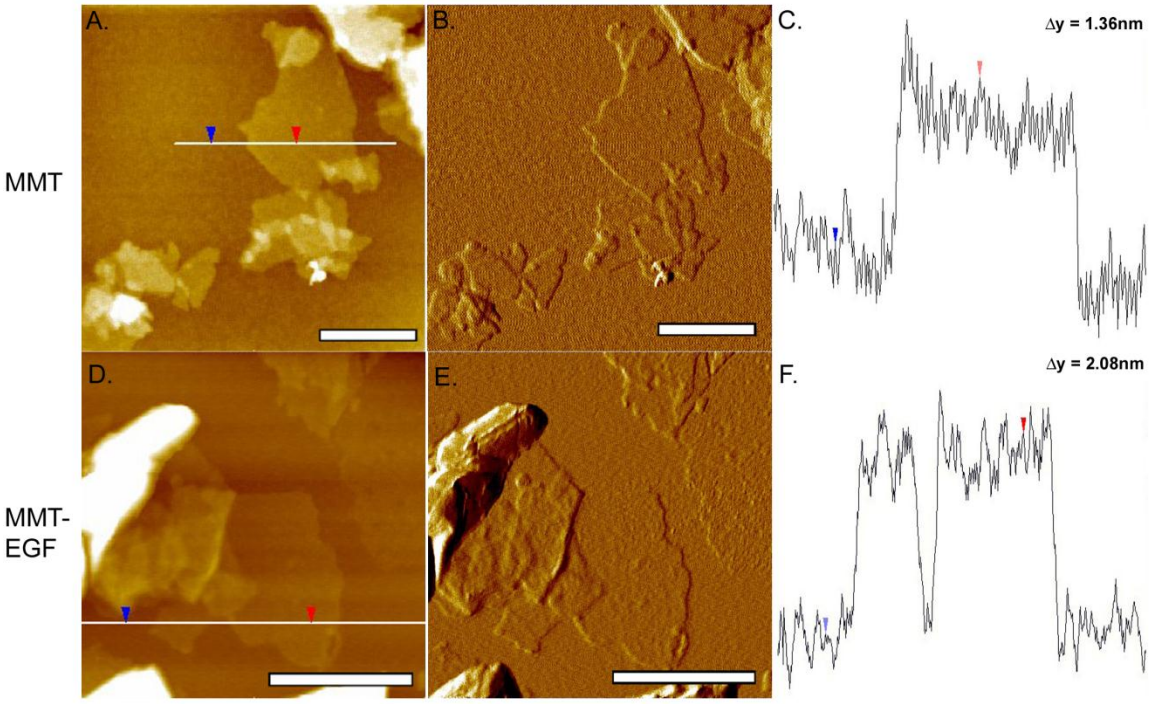
MMT
MMT-EGF
A.
B.
C.
Δy = 1.36nm
D.
E.
F.
Δy = 2.08nm

Figure 13. MMT-EGF is stable in cell culture media. A. Immunoblot analysis of Epilife complete media, 10 ng EGF, and fraction of a control MMT-EGF pellet. B. MMT-EGF was incubated at 37 ˚C and 5 % CO_2; the sample was washed, pelleted, and the supernatant collected to assay for unbound EGF every 24 hr up to 72 hr. C. Three independent EGF-MMT samples were incubated at 37 ˚C and 5 % CO_2 for 24, 48, and 72 hr; the sample was washed, pelleted, and the sup collected to assay for unbound EGF. Fractions of all pellets and controls were resolved on a 15 % SDS-PAGE and probed with anti-EGF antibodies.

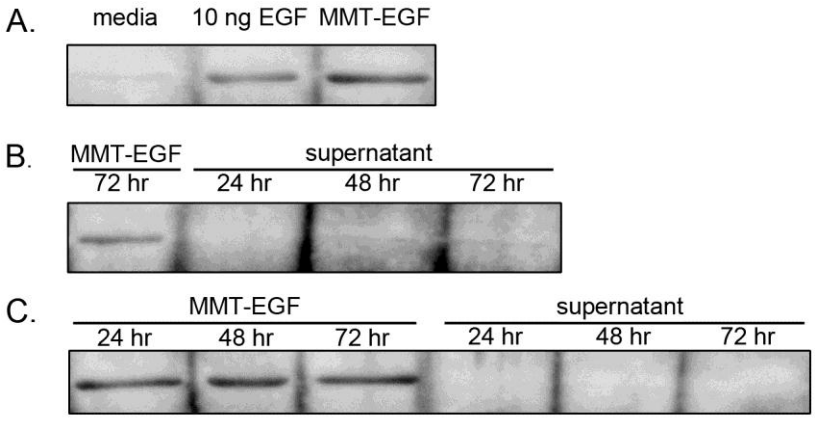
A.
media
10 ng EGF
MMT-EGF
B.
MMT-EGF
supernatant
72 hr
24 hr
48 hr
72 hr
C.
MMT-EGF
supernatant
24 hr
48 hr
72 hr
24 hr
48 hr
72 hr

EGF that remained bound to MMT. While much of the EGF remains in the MMT-EGF complex, trace amounts of EGF can be observed in the supernatant at 48 and 72 hr. Figure 13C shows three separate pellets incubated in the same conditions for 24, 48, and 72 hr, with a single wash and supernatant collection at each of the aforementioned time points. It can be seen that the MMT-EGF pellets remain intact and that no EGF is found in the supernatant, suggesting incubation and heating alone without periodic disturbance will not cause EGF to detach. The fact that EGF is bound so tightly to the MMT surface via electrostatic forces questions whether or not EGFR on the cell membrane can access EGF upon MMT-EGF treatment. It is known that EGFR consists of two inactive monomers that must bind two individual EGF ligands (or a potential EGF dimer) in order to autophosphorylate (Lu et al.). Restriction of EGF movement while bound to MMT may provide a challenge for the receptor to accomplish this.

E. Treatment of HaCaT cells with MMT-EGF leads to EGFR activation.

After verification that a low dose of MMT alone was nontoxic and EGF was present in the composite material, we next sought to determine if the MMT-EGF complex was biologically active. Upon ligand binding (EGF), EGF receptor (EGFR) forms a homodimer and autophosphorylates several tyrosine residues to form an active kinase. Activation of EGFR sends a global signal promoting migration, growth and survival (Marques et al.). In order to confirm activation of EGFR following MMT-EGF treatment of cells, we monitored EGFR activation

using phospho-specific antibodies to EGFR. Treatment with MMT alone led to no phosphorylation of EGFR as expected (Figure 14A). As shown in Figure 14B, treatment with either EGF or MMT-EGF led to phosphorylation of EGFR along the cell membrane as early as 30 min post-treatment. In a parallel experiment, full activation of EGFR by MMT-EGF was also observed at 120 min post-treatment as measured by immunoblot analysis as seen in Figure 14C. It remains unclear as to whether EGF is released from the clay surface or remains bound to MMT upon addition to cells, although results indicate minimal to no detectable detachment of EGF in culture media. This leads us to the hypothesis that an intact MMT-EGF complex activates EGFR at the cell surface.

Activated EGFR transmits a pro-growth signal to the cell through various signaling pathways, one major pathway being the phosphoinositide 3-kinase (PI3K)/AKT pathway (Dunker and Fernández). To assess whether MMT-EGF nanocomposites function in a similar fashion as EGF alone, we monitored AKT phosphorylation and its downstream target GSK3β at multiple time points after addition of EGF or MMT-EGF to serum starved cells. We observed that AKT activation occurs within 30 min in serum starved HaCaT cells treated with MMT-EGF as shown in Figure 15, which mirrors the result of EGF treatment alone. AKT activation leads to phopshorylation of several downstream targets, such as GSK3β, to promote cell survival (Vander Haar et al.; Jope and Johnson). We observed a conservative increase in GSK3β phosphorylation upon addition of MMT-EGF at time points consistent with, or slightly after, AKT

Figure 14. Confocal microscopy analysis of EGFR activation. A. HaCaT cells were plated on sterilized coverslips. At 24 hr post seeding, cells were subject to starvation with serum free DMEM for 24 hr, then fixed and stained for phospho-EGFR (green), and DAPI was used to stain the nuclei (blue) and imaged using confocal microscopy. Cells with no treatment or MMT treatment alone show no EGFR activation. Scale bar = 20 μm. B. Serum-starved HaCaT cells were maintained as described above and spiked with MMT-EGF or EGF for 30, 60, or 120 min before staining. C. In a parallel experiment, HaCaT cells were seeded and subject to starvation followed by EGF (5 ng/ml) or MMT-EGF (0.001 wt % MMT) treatment as previously described. Whole cell lysates were subjected to immunoblot analysis using antibodies specific for phospho-EGFR or β-actin as a loading control.

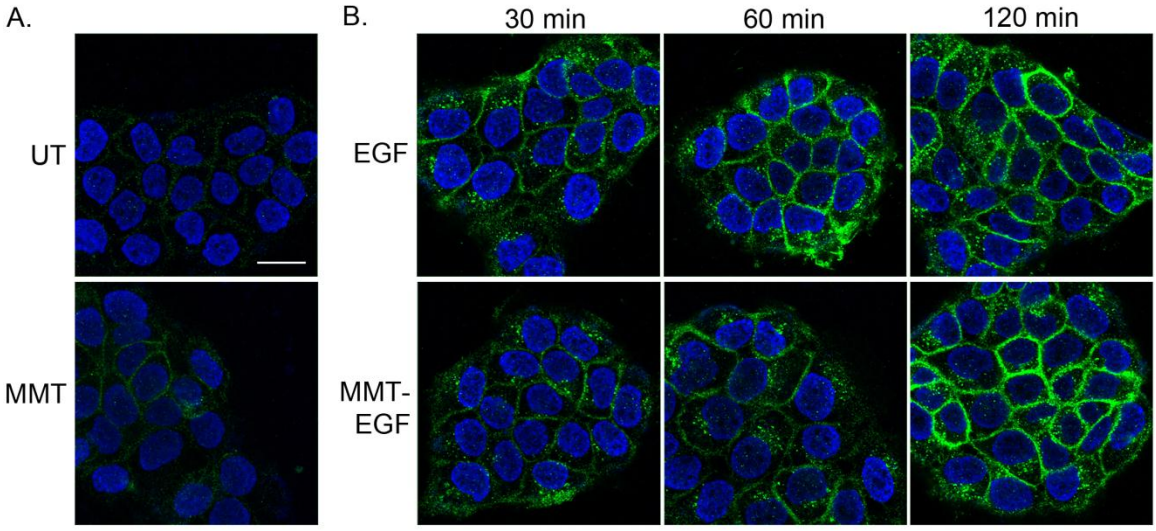
A.
B.
30 min
60 min
120 min
UT
EGF
MMT
MMT-
EGF

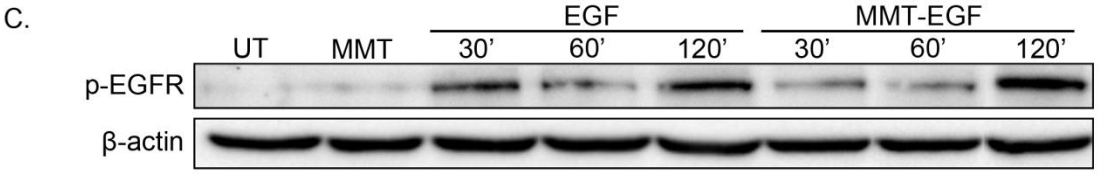
C.
EGF
MMT-EGF
UT
MMT
30’
60’
120’
30’
60’
120’
p-EGFR
β-actin

Figure 15. Activation of EGFR leads to AKT and ERK activation in HaCaT cells treated with MMT-EGF. HaCaT cells were serum starved for 24 hr. Cells were treated with 5 ng/mL EGF or 0.001 % MMT-EGF pre-equilibrated in serum free DMEM, and whole cell extracts were obtained at 30, 60, or 120 min. Whole cell lysates were subjected to immunoblot analysis for the indicated proteins. β-actin was used as a loading control.

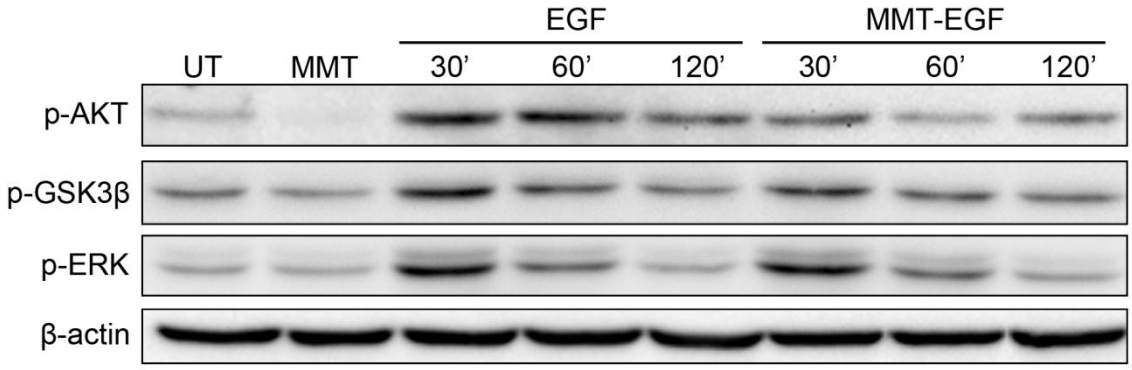
EGF
MMT-EGF
UT
MMT
30’
60’
120’
30’
60’
120’
p-AKT
p-GSK3β
p-ERK
β-actin

activation (Figure 15). EGFR also promotes cell growth by means of the mitogen activated protein kinase (MAPK) pathways such as ERK1/2 via the RAS-RAF-MEK cascade (Seger and Krebs). Therefore we monitored ERK activation in HaCaT cells treated with MMT-EGF and demonstrated that ERK phosphorylation occurs within 30 min following treatment with MMT-EGF as shown in Figure 15. Altogether these results indicate MMT-immobilized EGF induces activation of EGFR and subsequent downstream protein signaling events at a similar rate to EGF treatment alone.

F. MMT-EGF mediated increased cell migration of HaCaT is dependent on ERK activation.

Since MMT is thought to interact with the cell membrane, we next sought to determine if the presence of MMT wound inhibit the normal migratory response of HaCaT cells to EGF (Lordan, Kennedy and Higginbotham). Keratinocyte motility during wound healing is known to be regulated by ERK activity via the RAS-RAF-MEK cascade (Matsubayashi et al.). To monitor the effects of MMT-EGF on cell migration we performed *in vitro* scratch wound assays to determine cell migration across the “wound”. Figure 16A shows that MMT-EGF treatment induced cell migration at a rate comparable to that of EGF treatment alone, while treatment with MMT alone fails to induce cell migration. Quantitation of the wound closure rates showed that although the MMT-EGF shows an initial lag, a complete wound closure comparable to EGF alone was observed by 24 hr (Figure 16B). Altogether our results demonstrate that EGF

Figure 16. HaCaT migration in response to MMT-EGF treatment. A. HaCaT cells were grown to near confluence and then serum starved for 24 hr. A scratch wound was induced and cells were left untreated (UT) in serum free media, or treated with 0.001 % MMT, 0.01 % MMT-EGF or 5 ng/ml EGF for up to 24 hr. Images displayed are representative of three independent experiments. Scale bar = 100 µm. B. Quantification of scratch-wound closure is plotted as the average wound closure. Error bars represent the standard deviation between experiments.

A.

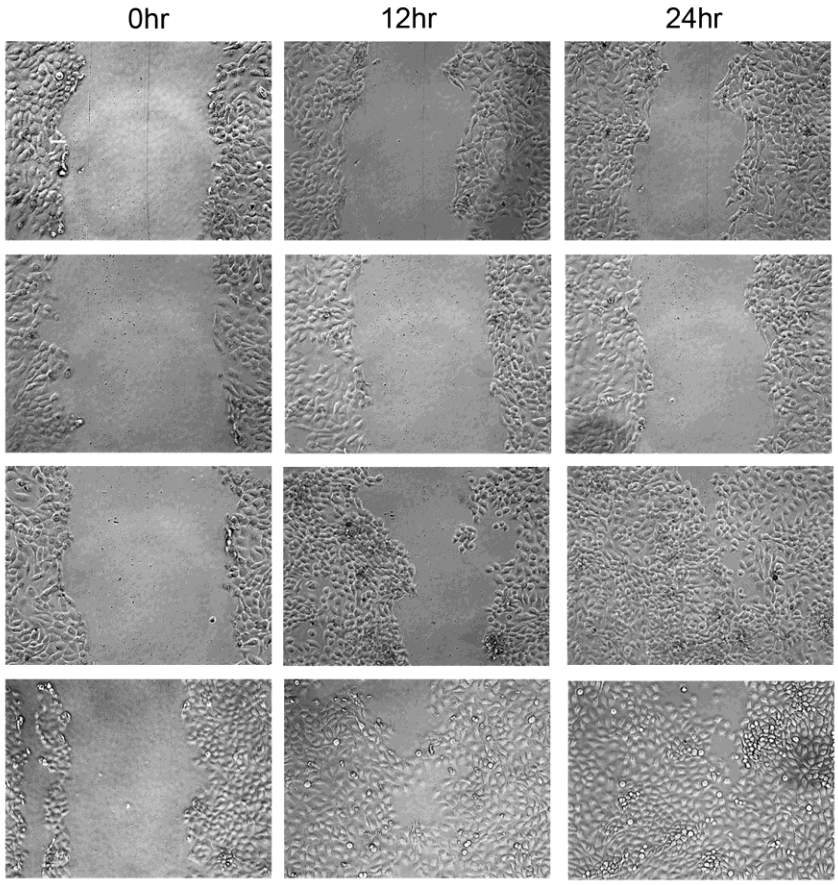
0hr
12hr
24hr
UT
MMT
MMT-EGF
EGF

B.

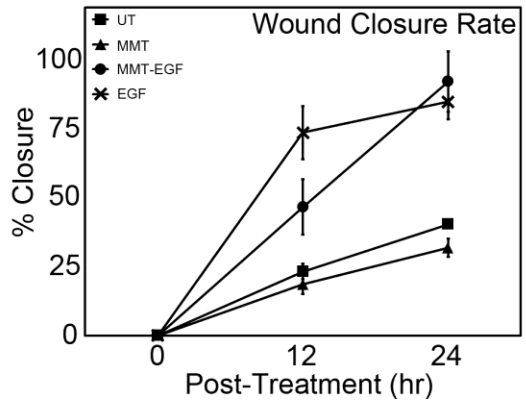
Wound Closure Rate
UT
MMT
MMT-EGF
EGF
% Closure
100
75
50
25
0
0
12
24
Post-Treatment (hr)

immobilized on the clay surface is active, can stimulate cell migration, and that the presence of MMT does not interfere with the cell movement. A similar migratory response is observed in IMR-90 cells with MMT-EGF treatment as seen in Figure 17. Although complete wound closure was not observed in either EGF or MMT-EGF treated cells, the cells responded to both EGF and MMT-EGF similarly.

To verify the regulation of MMT-EGF induced cell migration by the ERK pathway, we performed scratch wound assays after pre-treatment with RAPA or PD98059 to inhibit activities of the mTOR and MEK1 pathaways, respectively (Kaufmann and Thiel). The effectiveness of these inhibitors can be seen via Western Blot analysis as shown in Figure 18A. RAPA inhibits the kinase activity of mTOR Complex 1, which can be observed by the effective decrease in phosphorylation of S6 by S6 kinase, a downstream target of mTOR. PD98059 selectively binds activation sites of MEK1 (ERK kinase), inhibiting its kinase activity as observed by the decrease in phosphorylated ERK. As shown in Figure 18B, cells treated with RAPA displayed migration patterns similar to vehicle treated cells, suggesting that the activation of mTOR does not play a major role in MMT-EGF induced cell migration. In contrast, cells treated with PD98059 resulted in no cell movement after MMT-EGF treatment, suggesting that the ERK1/2 pathway plays a major role in MMT-EGF induced cell migration during wound healing, consistent with the normal response of HaCaT cells to EGF.

Figure 17. IMR-90 migration in response to MMT-EGF treatment. A. IMR-90 cells were seeded in 6-well plates in DMEM containing 10 % FBS and grown to near confluence, then subjected to starvation with serum-free DMEM for 24 hr. A scratch wound was induced and cells were left untreated (UT) in serum free media, or treated with .01 % MMT or MMT-EGF for up to 24 hr. Images displayed are representative of three independent experiments. Scale bar = 100 µm.

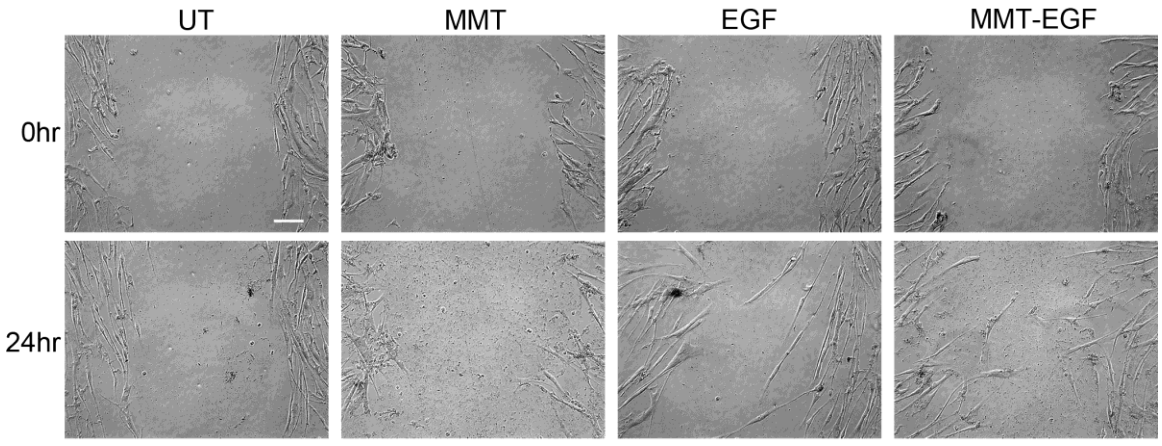
UT
MMT
EGF
MMT-EGF
0hr
24hr

Figure 18. Inhibition of MEK1 suppresses MMT-EGF induced cell migration. A. HaCaT cells were grown to near confluence and then serum starved for 24 hr. A scratch wound was induced and cells were pre-treated for 4 hr with 100 nM rapamycin (RAPA) or 75 µM PD98059 in DMSO, or equal volumes of control vehicle, then left untreated (UT) in serum free media, or treated with 0.001 % MMT-EGF for up to 24 hr. Scale bar = 100 µm. B. In a parallel experiment, HaCaT cells were serum starved for 24 hr. Cells were pre-treated for 4 hr with 100 nM RAPA or 75 µM PD98059, then treated with 5ng/mL EGF or 0.001 % MMT-EGF pre-equilibrated in serum free DMEM, and equivalent amounts of whole cell extracts were subjected to immunoblot analysis using antibodies specific for phospho-S6, total S6, phospho-ERK, and total ERK. β-actin was used as a loading control.

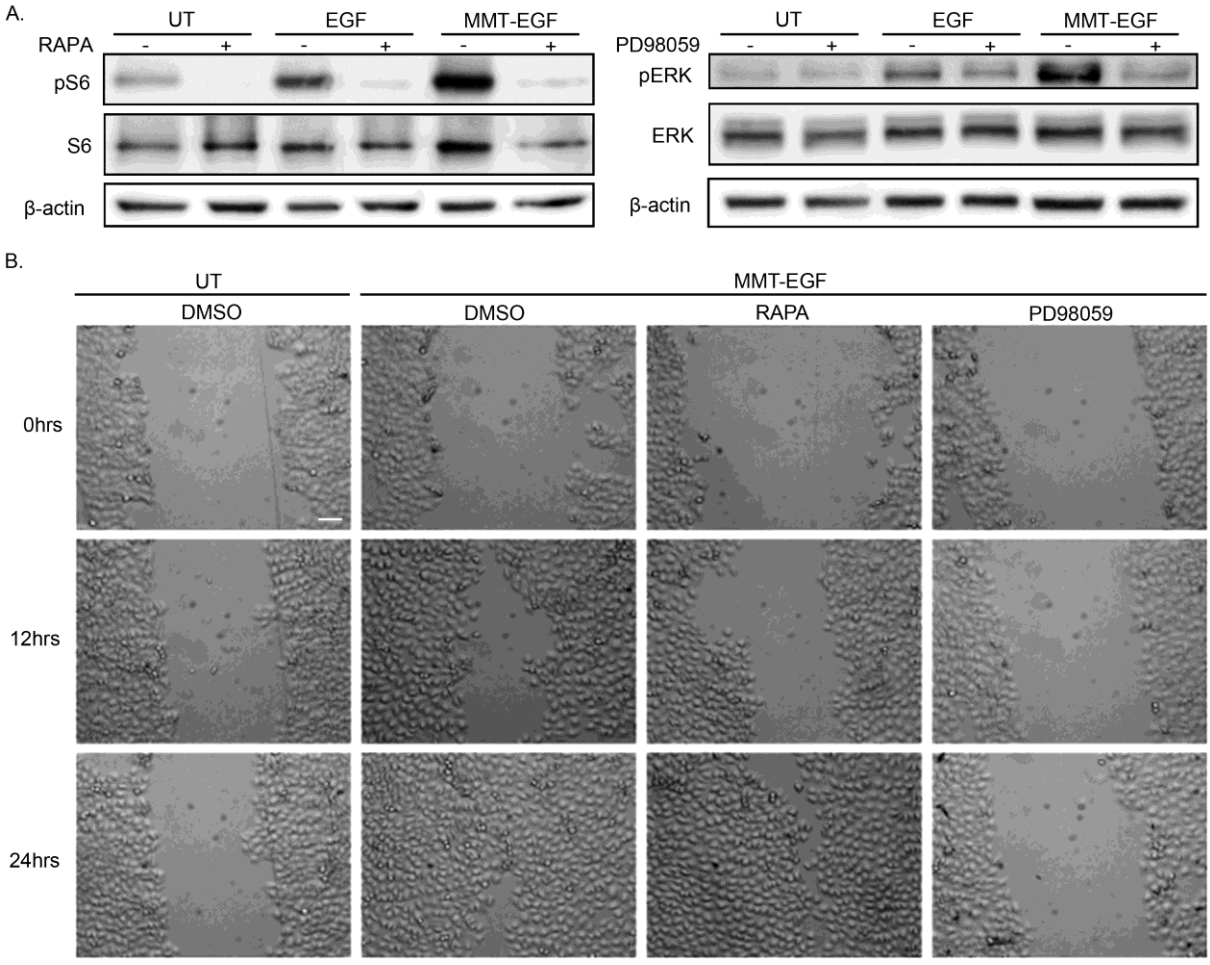
A.
UT
EGF
MMT-EGF
RAPA
- + - + - +
pS6
S6
β-actin
UT
EGF
MMT-EGF
PD98059
- + - + - +
pERK
ERK
β-actin
B.
UT
MMT-EGF
DMSO
DMSO
RAPA
PD98059
0hrs
12hrs
24hrs

We next examined the effects of MMT-EGF treatment on gene expression of THBS1, VEGF, and S100A shown to be involved in promoting cell growth in response to EGF treatment (Tong et al.; Stoll and Elder; Stoll, Zhao and Elder). The respective contribution of the mTOR and MEK1 pathways to gene induction was confirmed by treating cells with RAPA or PD98059 inhibitors prior to MMT-EGF treatment. As shown in Figure 19 MMT-EGF treatment leads to increased gene expression of THBS1, VEGF, and S100A2. Suppression of either the mTOR or MEK1 pathways by RAPA or PD98059, respectively, reduced MMT-EGF mediated induction of THBS1 and VEGF. Interestingly, MMT-EGF mediated upregulation of S100A2 expression was selectively blocked only by the MEK1 inhibitor PD98059 (Figure 19). S100A2 encodes CaN19, a calcium-binding protein involved in EGFR-triggered regenerative hyperplasia (Mischke et al.). These results are indicative of the important roles that the MEK1-ERK pathway plays in MMT-EGF induced keratinocyte migration and gene induction, thereby confirming that the MMT-EGF complexes activate the normal proliferative and migration signaling components of HaCaT cells.

Figure 19. **Expression of S100A2, VEGF, and THBS1 in response to MMT-EGF treatment.** HaCaT were serum starved for 24 hr, then pre-treated for 2 hr with 100 nM RAPA (R) or 75 µM PD98059 (PD), followed by treatment with 5 ng/mL EGF or 0.001% MMT-EGF (ME) pre-equilibrated in serum free DMEM. At 1 hr post-treatment RNA was harvested, cDNA made and quantitative real time PCR was performed to quantify transcript levels of S100A2, VEGF, and THBS1. Data is normalized to untreated cells (UT). (*$*p < 0.01, **p < 0.001, ***p < 0.0001$*, relative to EGF or ME treated cells using student's T-test). Real-time qRT-PCR experimentation and data analysis was conducted by Katie Leonard.

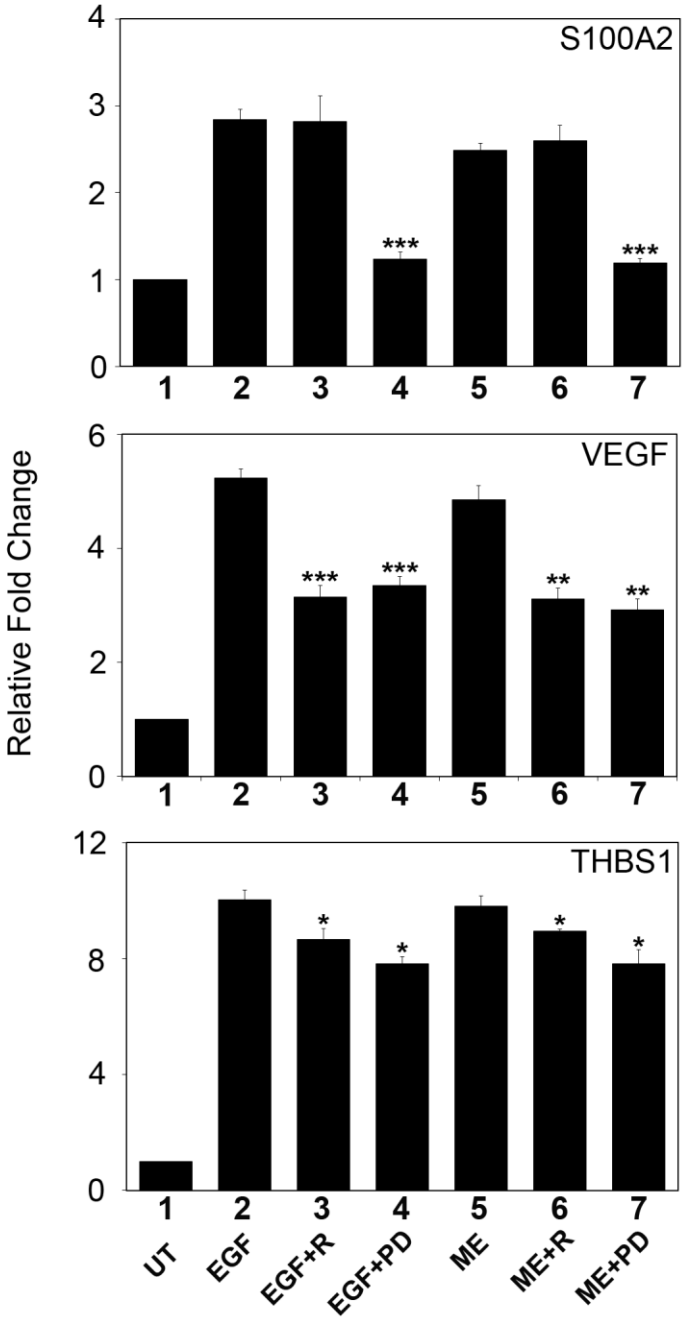
S100A2
VEGF
THBS1
Relative Fold Change
UT
EGF
EGF+R
EGF+PD
ME
ME+R
ME+PD

IV. Discussion

A. Bio-inorganic hybrid nanomaterials and their applications.

The field of polymer nanocomposites is a new and emerging technology that has already made a huge impact on material science. Lamellar materials such as MMT have seen industrial use in composite materials that date back to the1980s, when Toyota began to use clay platelets as a filler in several materials, and noticed a significant increase in tensile strength, flexibility, modulus, and heat resistance with such low loading amounts of clay (5 %) (Zhu and Wilkie). The ability to improve both strength and toughness was previously impossible with conventional technologies, and because of this polymer nanocomposites gained much industrial attention in areas like enhancing barrier properties and fire retardancy. More recently the study of natural and synthetic hybrid biomaterials has grown in the medical field with the development of implantations and prosthetics (Currie et al.). Current efforts in biological-inorganic hybrid materials have been seen in tissue engineering scaffolds and drug delivery (Tsuru, Hayakawa and Osaka). Porous silicate materials embedded with biological materials such as chitosan have been demonstrated to support cell growth and have become the centerpiece of many tissue engineering efforts. Understanding naturally occuring hybrid materials will aid in the development of constructing organic-inorganic hybrid materials *ex vivo*. One such example of a biological hybrid material is bone, a combination of organic collagen fibers and inorganic hydroxyapatite crystals. Understanding a system like the bone matrix

will improve the design of bio-inorganic materials, such as MMT-EGF as described in this study.

"Smart materials" are materials designed to physically or chemically respond to an environmental stimulus. Engineered smart materials containing biologically active components like enzymes have been widely explored for applications such as biocatalysis, medical implantation, and electrochemical sensors (Ritchie; Forano and Prévot). The use of glucose oxidase in the active layer of glucose sensors is a common example of exploiting the enzyme's natural specificity for diagnostic applications (Fujii, Hill and Ariga). Several challenges such as retention of biological activity and environmental stability necessitate the understanding of the interfacial interaction between the inorganic and biological material, in order to create a protective scaffold for the enzyme (Forano and Prévot). Herein, we briefly discuss the intercalation of HRP and GOX between lamellar MMT platelets. Preliminary results presented indicate a stabilization of HRP activity at a low pH that would normally render the enzyme inactive. While this serves as an adequate proof-of-concept for applications such as the oral or topical delivery of biological-inorganic materials to an aqueous environment, it does not address some of the main challenges associated with the non-aqueous use of biological-inorganic materials. However, the results presented within provide a foundation from which to build a more accurate model of protein-clay interfaces.

B. Clay nanomaterials for drug delivery applications.

The drug binding-release properties of many nanomaterials have been well classified and prove to be a promising route for the delivery of many chemotherapeutic agents. While not pursued fully in this study due to its weak interaction with EGF, halloysite nanotubular clay has been studied as a drug delivery vehicle in many research efforts both *in vitro* and *in vitro* (S. R. Levis and P. B. Deasy; Price, Gaber and Lvov; Lvov and Price). As an inexpensive and widely abundant natural material, halloysite nanotubes provide an advantage over similarly structured materials like carbon nanotubes for applications requiring biocompatible nano-scale carriers, such as drug delivery. Loading of the halloysite tubes with biomolecules usually includes solution mixing halloysite powder with the drug-containing solution, and decreasing the system's pressure using vacuum chambers to draw the water out of the tubes (Lvov and Price). Although the release properties of drug-loaded halloysite systems have been fairly well characterized, we chose not to further pursue this material for EGF mediated wound healing.

In this study we instead chose to develop MMT-EGF via ion exchange reaction, a procedure that does not require such equipment as vacuum chambers. The mechanism of charged clay particles as drug carriers via electrostatic forces is idealized by Aguzzi *et al*. as a two-step ion exchange reaction, the first step being the "loading" of the clay via ion exchange of the drug molecule onto the clay surface, and the second being the "delivery" as the drug exchanges off for ionic species in the environment (Aguzzi et al.). The release

mechanisms of drug-loaded MMT particles is observed with varying efficiencies and is dependent on the strength of the bond between MMT and the drug molecule, and the ionic conditions of the delivery environment. In some cases complete unloading of the MMT particle is not achieved, and release efficiencies are lower than 50 %, while others observe a slow but complete release of all molecules (G. V. Joshi et al.; Ghanshyam V. Joshi et al.; Chen et al.). Therefore it is accepted that in some cases, molecules will remain on the clay surface. While many drug-delivery studies focus on the release properties of clays, research groups using MMT in composite scaffolds recognize enhanced cell adhesion to clay-topped surfaces, and others analyzing MMT suspension in cell culture observe aggregation of clays onto the cell surface at high concentration with bright-field microscopy (Lordan, Kennedy and Higginbotham; Mehta et al.). This property may help draw MMT-EGF complexes to the cell membrane surface. In this study we have confirmed the binding of EGF to MMT via immunoblot analysis. The low-loading concentration of our reaction conditions allow for the majority of ion-exchange sites to continue to be occupied by Na^+, and results in little to no detectable intercalation of EGF within the interlayer space of dried MMT crystallite stacks. Here we observe a strong bond between EGF and MMT after several days of incubation in complete media, suggesting that MMT-EGF remains largely intact while no detectable EGF is released into the environment. This leads to our hypothesis of a direct delivery of intact MMT-EGF complexes to the cell membrane that might be beneficial for wound healing.

C. Growth factor therapy for wound healing.

The pros and cons of growth factor therapy for treating different types of wounds have been well reviewed (Hardwicke et al.). For example, Hardwicke *et al.* bring notice to the challenges associated with EGF treatment of chronic wounds, which include degradation by proteases of the protein upon treatment, and the need for protein modification or protective delivery systems to mitigate this response. Montmorillonite has previously been shown to enhance the thermal and pH stability of immobilized enzymes, suggesting a degree of protection from the environment provided by the clay (Sanjay and Sugunan). While not explored in this study, immobilization of EGF on the surface of MMT may offer a similar degree of protection from an environment containing proteolytic enzymes, and warrants future study. Several different delivery methods of EGF have been studied today, including electrospun nanofiber scaffolds conjugated with EGF for tissue repair of diabetic ulcers (Choi, Leong and Yoo). EGF treatment is commonly administered to patients with diabetic ulcers in gel or ointment form. Drawbacks of this treatment include a “burst” effect of EGF treatment, where EGF is consumed or destroyed soon after treatment, and frequent reapplication is necessary. This is a challenge that the studies on EGF conjugated nanofibers attempts to address. Another interesting study suggests that synthetic polymers found in artificial tears can activate EGFR and stimulate wound healing (Lozano et al.). Findings like this may spur research in wound treatment using synthetic materials, which would be significantly cheaper than human growth factors. Another reason to target EGFR

is for cancer therapies and imaging, since EGFR is overexpressed in many cancer cell lines (Zhang et al.). Magnetic nanoparticles conjugated with EGF have been shown to be taken up by the cancer cell line CaCo-2, suggesting a possible means for site-directed magnetic imaging of tumors (Creixell et al.). While advances in nanoparticle imaging systems for tumors have gained much ground in recent years, challenges such as the cytotoxicity of such imaging agents still must be overcome (Selvan et al.). Overall, EGFR is a powerful receptor, and understanding how to directly target EGFR will significantly impact the fields of wound healing, as well as the imaging and treatment of certain cancers.

Battlefield injury provides a unique situation where growth factors may be used to enhance existing or newly discovered hemostatic agents. Advanced cauterizing agents such as QuikClot^{TM} work extremely well to prevent blood loss, but result in significant burns and inhibited long-term tissue regeneration (Arnaud et al.). The battlefield wound first demands a rapid clotting ingredient, however as blood clotting treatments become more advanced and effective, long-term tissue regeneration also needs to be addressed. This study focuses on MMT, a layered silicate shown to have natural hemostatic properties, as a carrier for tissue regenerating growth factors. MMT-HRP was used as a model to verify the intercalation and retained biological activity of biomolecules on the surface of MMT. We then confirm EGF will also bind to MMT, and have shown that MMT-EGF will induce a signaling response in HaCaT cells, as summarized by Figure 20, at the genetic, protein, and cellular level to stimulate cell migration.

Figure 20. Schematic diagram of hypothesized MMT-EGF induced growth signaling in HaCaTs. A schematic representation of the hypothesized signal transduction mechanism and cellular effects in HaCaT cells treated with 0.001 % MMT-EGF as observed in this study. Tightly bound MMT-EGF complexes directly activate EGFR on the cell membrane, inducing activation of downstream signaling cascades leading to genetic upregulation and cell migration.

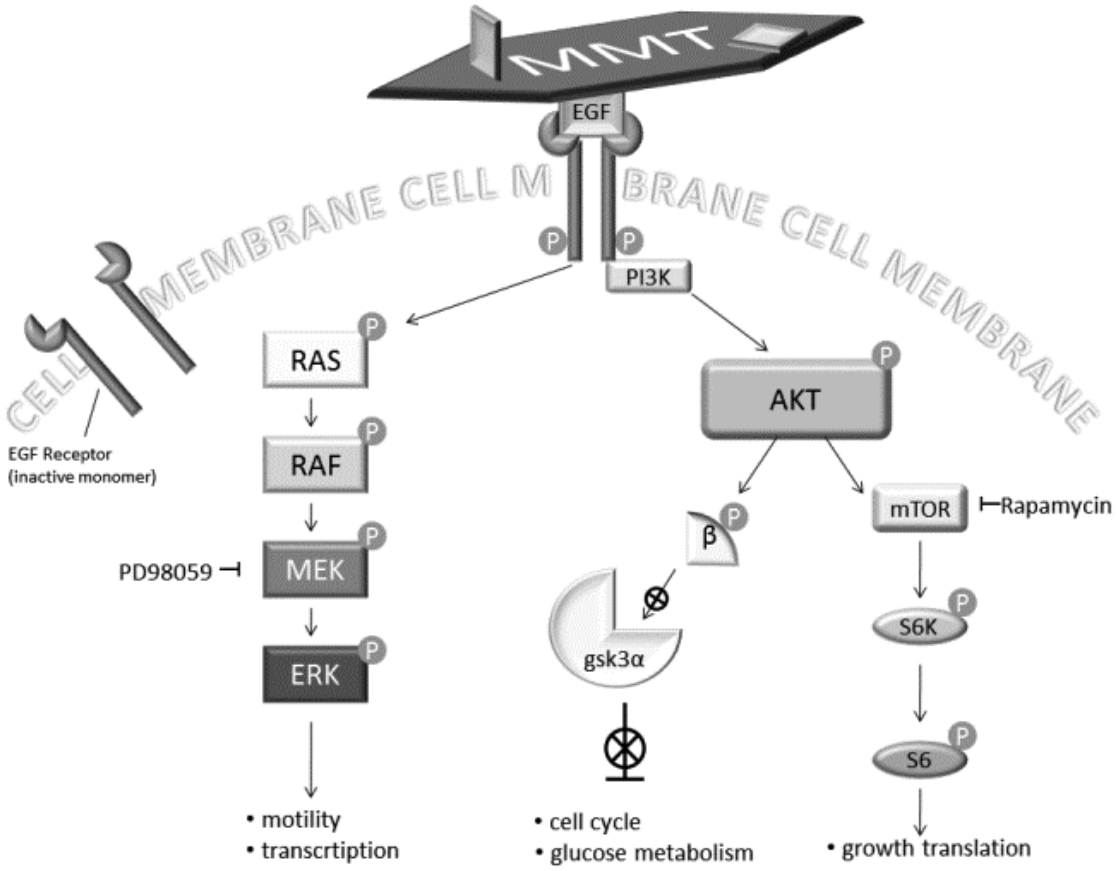
MMT
EGF
CELL MEMBRANE CELL M
BRANE CELL MEMBRANE
P
P
PI3K
RAS
RAF
MEK
ERK
PD98059
EGF Receptor
(inactive monomer)
AKT
β
gsk3α
mTOR
Rapamycin
S6K
S6
• motility
• transcrtiption
• cell cycle
• glucose metabolism
• growth translation

Confocal and immunoblot analysis confirm the successful activation of EGFR and subsequent signaling cascades following MMT-EGF treatment. This activation mirrors the effect of EGF treatment alone, suggesting no negative alteration of EGFR activation in the presence of MMT. Scratch wound assays confirm the ability of MMT-EGF to induce HaCaT cell migration, which is dependent on ERK activation, and also mirrors the normal activation pathway induced by EGF alone. Finally, the upregulation of a subset of pro-growth genes can be observed in response to MMT-EGF, following the same trend as cells treated with EGF alone. With EGF only occupying 0.01 % of the available Na^+ exchange sites, the MMT-EGF complex is predicted to maintain its ability to activate clotting factors such as Factor XII. Further investigation of the retained ability of EGF-bound MMT to induce coagulation is necessary. A better understanding of the binding and release properties of MMT-EGF would help determine the potential use of silicate-growth factor composites as a wound healing treatment.

V. References

Aguzzi, C., et al. "Use of Clays as Drug Delivery Systems: Possibilities and Limitations." *Applied Clay Science* 36.1-3 (2007): 22-36. Print.

Alam, H. B., et al. "Hemorrhage Control in the Battlefield: Role of New Hemostatic Agents." *Mil Med* 170.1 (2005): 63-9. Print.

Arnaud, F., et al. "Exothermic Reaction in Zeolite Hemostatic Dressings: Quikclot Acs and Acs+." *Ann Biomed Eng* 36.10 (2008): 1708-13. Print.

Baker, Sarah E., et al. "Controlling Bioprocesses with Inorganic Surfaces: Layered Clay Hemostatic Agents." *Chemistry of Materials* 19 (2007): 4390-92. Print.

Beanes, S. R., et al. "Skin Repair and Scar Formation: The Central Role of Tgf-Beta." *Expert reviews in molecular medicine* 5.8 (2003): 1-22. Print.

Berglund, G. I., et al. "The Catalytic Pathway of Horseradish Peroxidase at High Resolution." *Nature* 417.6887 (2002): 463-8. Print.

Bose, S., et al. "The Akt Pathway in Human Breast Cancer: A Tissue-Array-Based Analysis." *Modern pathology : an official journal of the United States and Canadian Academy of Pathology, Inc* 19.2 (2006): 238-45. Print.

Burnette, W. Neal. ""Western Blotting": Electrophoretic Transfer of Proteins from Sodium Dodecyl Sulfate-Polyacrylamide Gels to Unmodified Nitrocellulose and Radiographic Detection with Antibody and Radioiodinated Protein A." *Analytical Biochemistry* 112.2 (1981): 195-203. Print.

Chen, Youmei, et al. "Tramadol Hydrochloride/Montmorillonite Composite: Preparation and Controlled Drug Release." *Applied Clay Science* 49.3 (2010): 108-12. Print.

Choi, J. S., K. W. Leong, and H. S. Yoo. "In Vivo Wound Healing of Diabetic Ulcers Using Electrospun Nanofibers Immobilized with Human Epidermal Growth Factor (Egf)." *Biomaterials* 29.5 (2008): 587-96. Print.

Clay, J. G., J. K. Grayson, and D. Zierold. "Comparative Testing of New Hemostatic Agents in a Swine Model of Extremity Arterial and Venous Hemorrhage." *Mil Med* 175.4 (2010): 280-4. Print.

Cochrane, C. G., S. D. Revak, and K. D. Wuepper. "Activation of Hageman Factor in Solid and Fluid Phases. A Critical Role of Kallikrein." *J Exp Med* 138.6 (1973): 1564-83. Print.

Creixell, M., et al. "Preparation of Epidermal Growth Factor (Egf) Conjugated Iron Oxide Nanoparticles and Their Internalization into Colon Cancer." *Journal of Magnetism and Magnetic Materials* 322 (2010): 2244-50. Print.

Currie, Heather A., et al. *Natural and Artificial Hybrid Biomaterials*. Hybrid Materials: Wiley-VCH Verlag GmbH & Co. KGaA, 2007. Print.

Danielsen, A. J., and N. J. Maihle. "The Egf/Erbb Receptor Family and Apoptosis." *Growth Factors* 20.1 (2002): 1-15. Print.

Dunker, A. K., and A. Fernandez. "Engineering Productive Enzyme Confinement." *Trends in Biotechnology* 25.5 (2007): 189-90. Print.

Dunker, A. Keith, and Ariel Fernández. "Engineering Productive Enzyme Confinement." *Trends in Biotechnology* 25.5 (2007): 189-90. Print.

Ellis-Behnke, Rutledge G., et al. "Nano Hemostat Solution: Immediate Hemostasis at the Nanoscale." *Nanomedicine* 2 (2006): 207-15. Print.

Forano, Claude, and Vanessa Prévot. *Enzyme-Based Bioinorganic Materials*. Bio-Inorganic Hybrid Nanomaterials: Wiley-VCH Verlag GmbH & Co. KGaA, 2008. Print.

Fu, Xiaobing, et al. "Engineered Growth Factors and Cutaneous Wound Healing: Success and Possible Questions in the Past 10 Years." *Wound Repair and Regeneration* 13.2 (2005): 122-30. Print.

Fujii, Kazuko, Jonathan P. Hill, and Katsuhiko Ariga. *Biomimetic Nanohybrids Based on Organosiloxane Units*. Bio-Inorganic Hybrid Nanomaterials: Wiley-VCH Verlag GmbH & Co. KGaA, 2008. Print.

Ganguly, Anirban, Anil K. Bhowmick, and Yongjin Li. "Insights into Montmorillonite Nanoclay Based Ex Situ Nanocomposites from Sebs and Modified Sebs by Small-Angle X-Ray Scattering and Modulated Dsc Studies." *Macromolecules* 41.16 (2008): 6246-53. Print.

Garwood, G. A., M. M. Mortland, and T. J. Pinnavaia. "Immobilization of Glucose Oxidase on Montmorillonite Clay: Hydrophobic and Ionic Modes of Binding." *Journal of Molecular Catalysis* 22.2 (1983): 153-63. Print.

Gopinath, Sanjay, and Sankaran Sugunan. "Enzymes Immobilized on Montmorillonite K 10: Effect of Adsorption and Grafting on the Surface Properties and the Enzyme Activity." *Applied Clay Science* 35.1-2 (2007): 67-75. Print.

Grim, Ralph E. *Clay Mineralogy*. 2 ed. New York: McGraw-Hill, 1968. Print.

Gupta, M. K., et al. "Patterned Silk Films Cast from Ionic Liquid Solubilized Fibroin as Scaffolds for Cell Growth." *Langmuir* 23.3 (2007): 1315-9. Print.

Hardwicke, J., et al. "Epidermal Growth Factor Therapy and Wound Healing -- Past, Present and Future Perspectives." *The Surgeon* 6.3 (2008): 172-77. Print.

Hartmeier, Winfried. "Immobilized Biocatalysts -- from Simple to Complex Systems." *Trends in Biotechnology* 3.6 (1985): 149-53. Print.

Hennessy, B. T., et al. "Exploiting the Pi3k/Akt Pathway for Cancer Drug Discovery." *Nat Rev Drug Discov* 4.12 (2005): 988-1004. Print.

Hudson, L. G., and L. J. McCawley. "Contributions of the Epidermal Growth Factor Receptor to Keratinocyte Motility." *Microsc Res Tech* 43.5 (1998): 444-55. Print.

Jones, ME. "Analysis of Algebraic Weighted Least-Squares Estimators for Enzyme Parameters." *Biochem J* 288.2 (1992): 533-38. Print.

Jope, R. S., and G. V. Johnson. "The Glamour and Gloom of Glycogen Synthase Kinase-3." *Trends in biochemical sciences* 29.2 (2004): 95-102. Print.

Joshi, G. V., et al. "Montmorillonite as a Drug Delivery System: Intercalation and in Vitro Release of Timolol Maleate." *Int J Pharm* 374.1-2 (2009): 53-7. Print.

Joshi, Ghanshyam V., et al. "Montmorillonite Intercalated with Vitamin B1 as Drug Carrier." *Applied Clay Science* 45.4 (2009): 248-53. Print.

Kaufmann, K., and G. Thiel. "Epidermal Growth Factor and Thrombin Induced Proliferation of Immortalized Human Keratinocytes Is Coupled to the Synthesis of Egr-1, a Zinc Finger Transcriptional Regulator." *J Cell Biochem* 85.2 (2002): 381-91. Print.

Kharlampieva, Eugenia, et al. "Flexible Silk–Inorganic Nanocomposites: From Transparent to Highly Reflective." *Advanced Functional Materials* 20.5 (2010): 840-46. Print.

Koivisto, L., et al. "Hacat Keratinocyte Migration Is Dependent on Epidermal Growth Factor Receptor Signaling and Glycogen Synthase Kinase-3alpha." *Exp Cell Res* 312.15 (2006): 2791-805. Print.

Kommagani, R., et al. "P73 Is Essential for Vitamin D-Mediated Osteoblastic Differentiation." *Cell death and differentiation* 17.3 (2010): 398-407. Print.

Langlands, K., G. A. Down, and T. Kealey. "Id Proteins Are Dynamically Expressed in Normal Epidermis and Dysregulated in Squamous Cell Carcinoma." *Cancer Res* 60.21 (2000): 5929-33. Print.

Lemmon, M. A., et al. "Two Egf Molecules Contribute Additively to Stabilization of the Egfr Dimer." *EMBO J* 16.2 (1997): 281-94. Print.

Levis, S. R., and P. B. Deasy. "Characterisation of Halloysite for Use as a Microtubular Drug Delivery System." *International Journal of Pharmaceutics* 243.1-2 (2002): 125-34. Print.

Levis, S.R., and P.B. Deasy. "Characterisation of Halloysite for Use as a Microtubular Drug Delivery System." *International Journal of Pharmaceutics* 243 (2002): 125-34. Print.

Liang, P., et al. "Anti-Apoptotic Role of Egf in Hacat Keratinocytes Via a Pparbeta-Dependent Mechanism." *Wound Repair Regen* 16.5 (2008): 691-8. Print.

Lin, F. H., et al. "A Study of Purified Montmorillonite Intercalated with 5-Fluorouracil as Drug Carrier." *Biomaterials* 23.9 (2002): 1981-7. Print.

Linare, C. F., L. Afonso, and M. Rose-Brussin. "Modified Venezuelan Kaolin as Possible Antacid Drug." *Journal of Applied Sciences* 4.3 (2004): 472-76. Print.

Lordan, Sinéad, James E. Kennedy, and Clement L. Higginbotham. "Cytotoxic Effects Induced by Unmodified and Organically Modified Nanoclays in the Human Hepatic Hepg2 Cell Line." *Journal of Applied Toxicology* 31.1 (2011): 27-35. Print.

Lozano, Jennifer S., et al. "Activation of the Epidermal Growth Factor Receptor by Hydrogels in Artificial Tears." *Experimental Eye Research* 86 (2008): 500-05. Print.

Lozzi, I., et al. "Interaction of Horseradish Peroxidase with Montmorillonite Homoionic to Na+ and Ca2+: Effects on Enzymatic Activity and Microbial Degradation." *Soil Biology and Biochemistry* 33.7-8 (2001): 1021-28. Print.

Lu, H. S., et al. "Crystal Structure of Human Epidermal Growth Factor and Its Dimerization." *J Biol Chem* 276.37 (2001): 34913-7. Print.

---. "Crystal Structure of Human Epidermal Growth Factor and Its Dimerization." *The Journal of biological chemistry* 276.37 (2001): 34913-7. Print.

Lvov, Yuri M., and Ronald R. Price. *Halloysite Nanotubules, a Novel Substrate for the Controlled Delivery of Bioactive Molecules*. Bio-Inorganic Hybrid Nanomaterials: Wiley-VCH Verlag GmbH & Co. KGaA, 2008. Print.

Madison, K. C. "Barrier Function of the Skin: "La Raison D'etre" of the Epidermis." *J Invest Dermatol* 121.2 (2003): 231-41. Print.

Marques, M. M., et al. "Egfr Family-Mediated Signal Transduction in the Human Keratinocyte Cell Line Hacat." *Exp Cell Res* 252.2 (1999): 432-8. Print.

Martin, P. "Wound Healing--Aiming for Perfect Skin Regeneration." *Science* 276.5309 (1997): 75-81. Print.

Matsubayashi, Y., et al. "Erk Activation Propagates in Epithelial Cell Sheets and Regulates Their Migration During Wound Healing." *Curr Biol* 14.8 (2004): 731-5. Print.

Mehta, G., et al. "Polyelectrolyte-Clay-Protein Layer Films on Microfluidic Pdms Bioreactor Surfaces for Primary Murine Bone Marrow Culture." *Advanced Functional Materials* 17.15 (2007): 2701-09. Print.

Michaelis, L, and ML Menten. "Die Kinetik Der Invertinwirkung." *Biochem. Z.* 49 (1913): 333-69. Print.

Mischke, D., et al. "Genes Encoding Structural Proteins of Epidermal Cornification and S100 Calcium-Binding Proteins Form a Gene Complex ("Epidermal Differentiation Complex") on Human Chromosome 1q21." *J Invest Dermatol* 106.5 (1996): 989-92. Print.

Ogiso, Hideo, et al. "Crystal Structure of the Complex of Human Epidermal Growth Factor and Receptor Extracellular Domains." *Cell* 110.6 (2002): 775-87. Print.

Pfaffl, M.W. "A New Mathematical Model for Relative Quantification in Real-Time Pcr." *Nucleic Acids Research* 29 (2001): 2002-07. Print.

Price, R. R., B. P. Gaber, and Y. Lvov. "In-Vitro Release Characteristics of Tetracycline Hcl, Khellin and Nicotinamide Adenine Dineculeotide from Halloysite; a Cylindrical Mineral." *Microencapsulation* 18.6 (2001): 713-22. Print.

Ritchie, Jason E. *Electronic and Electrochemical Applications of Hybrid Materials*. Hybrid Materials: Wiley-VCH Verlag GmbH & Co. KGaA, 2007. Print.

Sanjay, G., and S. Sugunan. "Enhanced Ph and Thermal Stabilities of Invertase Immobilized on Montmorillonite K-10." *Food Chemistry* 94 (2004): 573-79. Print.

Seger, R., and E. G. Krebs. "The Mapk Signaling Cascade." *The FASEB journal : official publication of the Federation of American Societies for Experimental Biology* 9.9 (1995): 726-35. Print.

Selvan, Subramanian Tamil, et al. "Functional and Multifunctional Nanoparticles for Bioimaging and Biosensing." *Langmuir* 26.14 (2009): 11631-41. Print.

Sharma, G. D., J. He, and H. E. Bazan. "P38 and Erk1/2 Coordinate Cellular Migration and Proliferation in Epithelial Wound Healing: Evidence of Cross-Talk Activation between Map Kinase Cascades." *J Biol Chem* 278.24 (2003): 21989-97. Print.

Simman, R., C. Craft, and B. McKinney. "Improved Survival of Ischemic Random Skin Flaps through the Use of Bone Marrow Nonhematopoietic Stem Cells and Angiogenic Growth Factors." *Ann Plast Surg* 54.5 (2005): 546-52. Print.

Singer, A. J., and R. A. Clark. "Cutaneous Wound Healing." *N Engl J Med* 341.10 (1999): 738-46. Print.

Stadelmann, W. K., A. G. Digenis, and G. R. Tobin. "Physiology and Healing Dynamics of Chronic Cutaneous Wounds." *Am J Surg* 176.2A Suppl (1998): 26S-38S. Print.

Stoll, S. W., and J. T. Elder. "Differential Regulation of Egf-Like Growth Factor Genes in Human Keratinocytes." *Biochem Biophys Res Commun* 265.1 (1999): 214-21. Print.

Stoll, S. W., X. Zhao, and J. T. Elder. "Egf Stimulates Transcription of Can19 (S100a2) in Hacat Keratinocytes." *J Invest Dermatol* 111.6 (1998): 1092-7. Print.

Tong, Q., et al. "Vegf Is Upregulated by Hypoxia-Induced Mitogenic Factor Via the Pi-3k/Akt-Nf-Kappab Signaling Pathway." *Respir Res* 7 (2006): 37. Print.

Tsuru, Kanji, Satoshi Hayakawa, and Akiyoshi Osaka. *Medical Applications of Hybrid Materials*. Hybrid Materials: Wiley-VCH Verlag GmbH & Co. KGaA, 2007. Print.

van den Helder, C. J., and J. J. Hage. "Sense and Nonsense of Scar Creams and Gels." *Aesthetic Plast Surg* 18.3 (1994): 307-13. Print.

Vander Haar, E., et al. "Insulin Signalling to Mtor Mediated by the Akt/Pkb Substrate Pras40." *Nature cell biology* 9.3 (2007): 316-23. Print.

Veitch, Nigel C. "Horseradish Peroxidase: A Modern View of a Classic Enzyme." *Phytochemistry* 65 (2004): 249-59. Print.

Wald, A. "Constipation, Diarrhea, and Symptomatic Hemorrhoids During Pregnancy." *Gastroenterol Clin North Am* 32.1 (2003): 309-22, vii. Print.

Zeineldin, Reema, and Laurie G. Hudson. *Epidermal Growth Factor: Methods and Protocols*. Methods in Molecular Biology. Ed. T. B. Patel, P. J. Bertics. Vol. 327. Totowa, NJ: Humana Press Inc, 2006. Print.

Zhang, H., et al. "Erbb Receptors: From Oncogenes to Targeted Cancer Therapies." *J Clin Invest* 117.8 (2007): 2051-8. Print.

Zhang, X., C. B. Baughman, and D. L. Kaplan. "In Vitro Evaluation of Electrospun Silk Fibroin Scaffolds for Vascular Cell Growth." *Biomaterials* 29.14 (2008): 2217-27. Print.

Zhu, Jin, and Charles A. Wilkie. *Intercalation Compounds and Clay Nanocomposites*. Hybrid Materials: Wiley-VCH Verlag GmbH & Co. KGaA, 2007. Print.